Spectral Analysis of Far-UV Galaxies With HST/COS Data

Naunet Leonhardes-Barboza*
2021 Physics REU, University of California, Santa Barbara

Faculty Advisor: Crystal Martin
University of California, Santa Barbara

(Dated: October 21, 2021)

We studied low mass galaxies that are growing rapidly, rare objects thought to be local analogs of the young galaxies that the James Webb Space Telescope will unveil at high redshift. Emission lines from these galaxies reveal physical properties in the star-forming regions, but the properties of the diffuse gas that accounts for most of the baryonic mass remain largely unconstrained. We examined 45 ultraviolet spectra obtained with the Hubble Space Telescope and looked for absorption lines from diffuse gas against the galaxy continuum. We identified 17 galaxies with very broad Lyman-alpha absorption wings, the damped Lyman alpha absorbers (DLAs). Here we describe how we fit the shape of these damped line profiles, a task complicated by blended metal line absorption, damped Milky Way H I absorption, and residual Lyman-alpha emission. The shape of the line wings is sensitive to the H I column density along the sight line. We find H I column densities ranging from 20.06 to 21.90, values comparable to the H I column through the disk of large galaxies like the Milky Way. Large H I columns in low mass galaxies are unusual. These H I column densities will be compared to the column densities of metal lines in future work. The resulting chemical enrichment of the diffuse gas will provide information about the physical origin of the DLA absorption. We also discuss the line profile of the residual Lyman-alpha after subtraction of the fitted DLA profile.

I. INTRODUCTION

Prior to the EoR, the universe consisted of a neutral hydrogen gas, and it is thought that the first stars and galaxies drove the reionization of said gas, "allowing the universe to begin to shine its first light" [1]. The study of nearby star-forming galaxies gives us insight into the structure of the early star-forming galaxies that drove the Epoch Of Reionization (EoR). In this paper, we investigate the properties of Lyman-alpha emission and absorption in a subset of the the CLASSY (Berg et al 2021; James et al 2021) spectra. These galaxies host young, compact star clusters with extreme damped Lyman Alpha absorption, troughs that are much broader and deeper than stellar population synthesis models can explain.

We model the continuum level underneath the Lyman-alpha emission-line profile. We show how the continuum model affects the subsequent Lyman-alpha emission-line profile. Accurate modeling of these DLAs strongly affects the subsequent emission-line modeling. Properties of the Lyman-alpha emission such as the peak-to-peak velocity separation provide a good indication of which galaxies leak Lyman continuum radiation, thereby contributing to the ionization of the IGM (REF Izotov; REF Jaskot).

The broad wings indicate high HI column densities, or Damped Lyman Alpha absorbers (DLAs), so they are also of scientific interest in their own right.

TABLE I: Galaxies with Damped Lyman Alpha Absorption In Survey.

Galaxy Name	z
J0127-0619	0.005400
J0144+0453	0.005200
J0337-0502	0.013520
J0405-3648	0.002800
J0823+2806	0.047223
J0934+5514	0.002500
J0940+2935	0.001675
J1044+0353	0.012870
J1105+4444	0.021540
J1129+2034	0.004703
J1132+1411	0.017637
J1132+5722	0.005041
J1150+1501	0.002448
J1225+6109	0.002341
J1444+4237	0.002300
J1448-0110	0.027412

For example, previous studies considered the HII region abundances when measuring the metal content of these galaxies, specifically the ratio of ionized oxygen abundances to hydrogen [2]. We can use DLA HI columns to examine the neutral, diffuse HI regions for an accurate view of the metal abundances in the neutral interstellar medium (ISM) [2]. The combined results provide a more complete census of the galaxies' star formation histories, accounting for all the metals (atomic number $Z > 2$ elements) produced by previous generations of stars.

* Also at Wellesley College

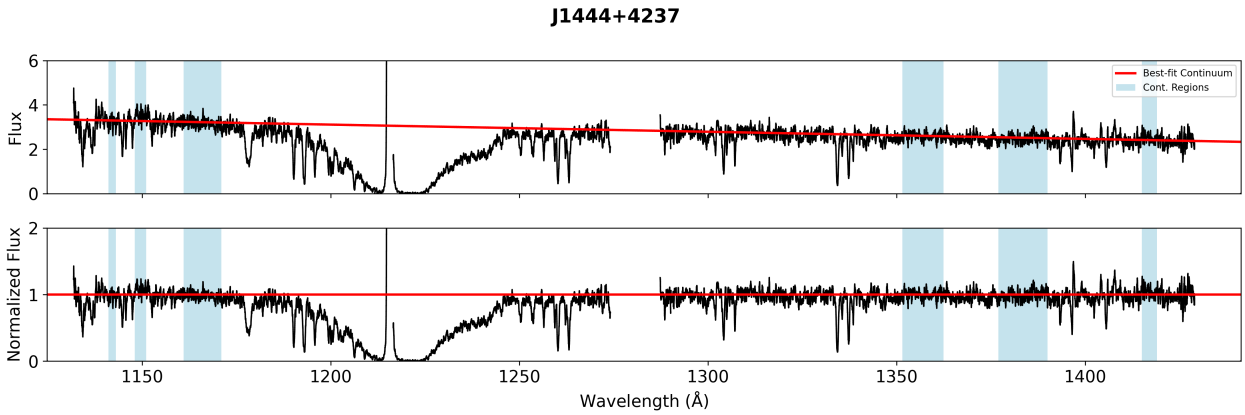

FIG. 1: Galaxy J1444+4237 with z = 0.002300. Spectral data smoothed for visual purposes. Red line is the best fit line. Blue areas are chosen continuum regions. Top plot shows the observed flux spectrum. Bottom plot shows the normalized flux spectrum..

II. METHODS

In this study, we investigate 15 low-redshift and low-metallicity galaxies in the far-ultraviolet from 1100-1450 Å listed in Table 1. We used spectra available from the Cosmic Origins Spectrograph (COS) aboard the Hubble Space Telescope. We smoothed these spectra by 18 pixels to better identify locations of possible absorption lines. When line-fitting, we use unbinned spectral data, so there is no additional covariance introduced between pixels. We use the python package VoigtFit [3] which takes the instrumental response function into account.

A. Continuum Normalization

By careful observation, we chose regions of each galaxy's spectrum to use as the continuum level in a linear fit. The continuum regions chosen for each galaxy in this study can be found in Table **??** in the appendix. We looked for regions that were 1) most unaffected by contamination from absorption or emission, 2) smaller error bars that could indicate the true continuum level, and 3) far from the broad damping wings of galaxy's Lyα trough. Then, we divide the raw flux and error by this best fit line to obtain the normalized flux and error for each spectrum, as shown for J1444+4237 in Fig. 1.

B. Masks

In order to accurately obtain absorption line profiles for each spectra, we chose to mask certain areas, or ignore them when running the fitting program.

Masks were applied when: 1) observed emission above the continuum level could be related to the source or geocoronal emission, 2) significant PCygni variable star absorption and emission region which is around NV 1242 and NV 1258 for the source (typically found in the red damping wing of Lyα trough), 4) detector gaps in the data, 5) unidentified absorption profiles, and 6) unphysical high flux at wavelengths below 1100 Å for affected spectra due to COS low sensitivity in that range.

We ran separate fits each with a different mask for the source's Lyα region that extend for a range of -400 to 1500 km s^{-1}, -400 to 2000 km s^{-1}, and one that did not mask this range. Our motivation for obtaining data from these differently masked fits are to account for hidden Lyα emission that could extend out to 2000 km s^{-1} into the blue wing of the deep trough. We want to examine how these different masks result in different HI column densities for the galaxy.

However, the approach to applying these masks changed from spectrum to spectrum. If there was extreme Lyα emission visibly seen in the spectrum, that was always masked among the 1500 km s^{-1}, 2000 km s^{-1}, and non-extended masked fit. Another issue that arose was that extending to -400 km s^{-1} from the galaxy's Lyα often ran into the geocoronal emission at Lyα's rest wavelength, therefore we would be fitting a spectra where we essentially masked out the entire bottom of the trough. Similarly in cases of extreme PCygni NV absorption-emission profiles, the extension of the Lyα mask out to 1500 or 2000 km s^{-1} would thereby mask the entire red wing of the trough as well. For these reasons, we were unable to run fits with certain spectra using the 1500 km s^{-1} and 2000 km s^{-1} masks, and we got inconsistent results from VoigtFit where we had to fix parameters of other ions to obtain a fit.

C. Absorption Line Fitting

We used the python package, VoigtFit, to create these multi-absorption line profiles. VoigtFit uses the equation

that describes the optical depth τ of an absorption line of transition i and element X by the column density of element X along with set of atomic parameters of line strength f_i, the damping constant Γ, and the resonance wavelength λ_i:

$$\tau_{i,X}(\lambda) = K_i \; N_X \; a_i \; H[a_i, x(\lambda)] \tag{1}$$

where K_i and a_i are given by:

$$\mathrm{K}_i = \frac{e^2\sqrt{\pi} f \lambda_i}{m_e c b} \qquad a_i = \frac{\lambda_i \Gamma_i}{4\pi b} \tag{2}$$

where e is the elementary charge, c is the speed of light, m_e is the electron mass, and b is the broadening parameter. This function also uses the analytical approximation of the Voigt-Hjerting function by Tepper-Garcia (2006) to get the line profile of a certain region:

$$H(a_i, x) \approx h - \frac{a_i}{x^2\sqrt{\pi}}[h^2(4x^4 + 7x^2 + 4 + 1.5x^{-2}) - 1.5x^{-2} - 1] \tag{3}$$

where $h = e^{-x^2}$.

We fit spectra using a simple two velocity-component model, where we input initial guesses for the velocity offset, b-parameter, and column density for each ion's component. For accurate spectral resolution, we use the extended source convolution of the COS G130M point-source line-spread function for each galaxy.

For spectra that contain blending of both MW H I and the source's Lyα trough, we fixed the MW H I component using column densities found from the Hartmann HI Atlas, a method found in this paper [2]. We ran different fits using a fixed versus free MW H I component as seen in **??**. In blended spectra, discrepancy between the two outputted MW H I column densities from the fixed versus free fit can be understood. However, the difference between these MW H I column densities in spectra where the MW H I and source HI trough are not blended can give insight on the error of our source's calculated column densities. This is further discussed in the Results section.

The biggest contamination of the red wing was the stellar winds from the source galaxy at N V 1238 and 1242.8 which would showcase a broad absorption feature immediately followed by an broad emission peak. Other transition lines that blended with the wings include: Si III 1206; Si II 1190.4, 1193.3, and 1260.4; N I 1199.6, 1200.2, and 1200.7; and S II 1250.6, 1253.8, and 1259.5. MW lines blended into the wings of the source's damped Lyman Alpha trough as well as blended with the galaxy's lines leading to complex absorption features.

We found visually that in order to get the best fit for the blue damping wing of the HI trough, fitting Si III seemed to be fundamental in improving the shape of the blue damping wing. For difficult weaker/highly contaminated lines like Si III or S II where VoigtFit outputted inconsistent results, we would fix the velocity offset and b-parameter to obtain a decent fit for the line. The velocity offset was fixed to be as close to the center of the absorption line as possible and b-parameter was changed by trial-and-error based on improved line shape from run to run. For some galaxies, the velocity offsets for several ions were fixed due to inconsistency of VoigtFit outputs.

D. Spectral Resolution

For accurate line fitting, the spectral resolution for the COS spectra is found using the line-spread function tables (LSF) provided at STSCI. These well-studied point-source LSFs (PSFs) were then convolved with the UV surface brightness profile of each galaxy to create unique extended-source LSFs (ESFs). We used these ESFs to obtain the correct spectral resolution for line-profile fitting. We output line profile fits using both LSFs (when possible) for comparison, and concluded that the ESF produces better, more consistent fits for each spectra. We see this visually in Fig. 2.

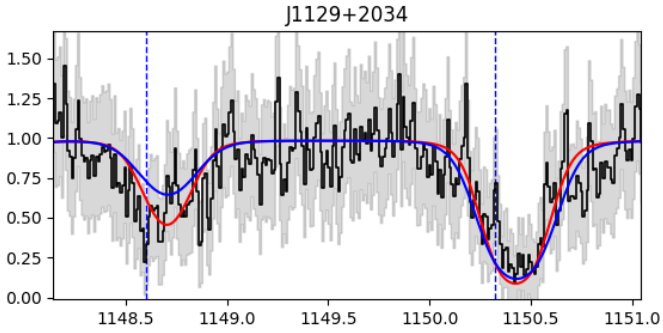

FIG. 2: Galaxy J1129+2034 with z = 0.004703. Source component of Fe II 1143 and 1144. Y-axis is normalized flux and x-axis is wavelength in Å. Blue dashed lines are the rest wavelength for the source. Black line is spectral data. The red line is the ESF, and the blue line is the PSF. In this example, we observe that the ESF passes through the spectral data and fits the wings of absorption features better than the PSF.

III. RESULTS

In this section, we describe the errors found in fitting each of the galaxies in our sample. The results for each galaxy lay the groundwork for fitting radiative transfer models to the Lyman alpha emission-line profile, a widely used diagnostic of Lyman continuum escape fraction and galactic outflows. It also enables a study of chemical

TABLE II: HI Column Densities For Source And Milky Way Component.

Object	redshift (z)		Source			Milky Way		
			Unextended	Extended 1500 km s^{-1}	Extended 2000 km s^{-1}	Unextended	Extended 1500 km s^{-1}	Extended 2000 km s^{-1}
J0127-0619	0.005400	Fixed	21.311 ± 0.009	-	-	-	20.612	-
		Free	21.210 ± 0.011	-	-	20.831 ± 0.017	-	-
J0144+0453	0.0052	Fixed	20.316 ± 0.008	20.069 ± 0.024	20.062 ± 0.027	-	20.540	-
		Free	20.324 ± 0.009	20.056 ± 0.029	20.048 ± 0.032	20.508 ± 0.011	20.550 ± 0.011	20.551 ± 0.011
J0337-0502	0.01352	Fixed	21.899 ± 0.002	21.909 ± 0.002	21.908 ± 0.002	-	20.566	-
J0405-3648	0.0028	Free	20.854 ± 0.008	21.010 ± 0.007	21.042 ± 0.008	20.376 ± 0.025	19.210 ± 0.183	18.821 ± 0.576
J1044+0353	0.01287	Fixed	21.879 ± 0.005	21.855 ± 0.004	21.858 ± 0.004	-	20.576	-
		Free	21.907 ± 0.005	21.871 ± 0.005	21.849 ± 0.005	20.401 ± 0.025	20.495 ± 0.021	20.591 ± 0.019
J0934+5514	0.0025	Fixed	21.314 ± 0.001	21.323 ± 0.001	21.331 ± 0.001	-	20.408	-
J0940+2935	0.001675	Fixed	21.363 ± 0.004	21.375 ± 0.004	21.393 ± 0.004	-	20.231	-
		Free	21.265 ± 0.013	21.322 ± 0.012	21.392 ± 0.011	20.845 ± 0.032	20.663 ± 0.053	20.266 ± 0.131
J1105+4444	0.02154	Fixed	21.478 ± 0.004	21.488 ± 0.004	21.508 ± 0.005	-	20.566	-
J1129+2034	0.004703	Fixed	21.233 ± 0.005	21.249 ± 0.005	21.275 ± 0.005	-	20.175	-
		Free	21.255 ± 0.006	21.277 ± 0.006	21.318 ± 0.006	19.984 ± 0.032	19.848 ± 0.041	19.593 ± 0.068
J1132+1411	0.017637	Fixed	20.688 ± 0.009	20.714 ± 0.011	20.722 ± 0.013	-	20.537	-
		Free	20.662 ± 0.010	20.678 ± 0.012	20.674 ± 0.011	20.683 ± 0.013	20.616 ± 0.015	20.618 ± 0.014
J1150+1501	0.002448	Fixed	21.086 ± 0.004	21.111 ± 0.005	21.138 ± 0.005	-	20.523	-
		Free	20.886 ± 0.013	21.082 ± 0.008	21.151 ± 0.008	21.018 ± 0.014	20.622 ± 0.021	20.518 ± 0.036
J1225+6109	0.002341	Fixed	21.378 ± 0.004	21.384 ± 0.004	21.400 ± 0.005	-	20.187	-
		Free	21.339 ± 0.010	21.359 ± 0.008	21.405 ± 0.008	20.620 ± 0.029	20.452 ± 0.046	20.143 ± 0.096
J1359+5726	0.033829	Fixed	20.719 ± 0.008	20.800 ± 0.008	20.816 ± 0.009	-	20.138	-
		Free	20.734 ± 0.008	20.790 ± 0.008	20.850 ± 0.007	20.118 ± 0.012	20.124 ± 0.007	20.121 ± 0.012
J1444+4237	0.0023	Fixed	21.598 ± 0.003	21.598 ± 0.003	21.599 ± 0.003	-	20.109	-
		Free	21.596 ± 0.009	21.597 ± 0.007	21.597 ± 0.008	20.494 ± 0.046	20.184 ± 0.141	20.208 ± 0.175
J1448-0110	0.027412	Fixed	21.614 ± 0.004	21.617 ± 0.004	21.623 ± 0.004	-	20.589	-

Notes. J0823+2806 and J1132+5722 are omitted because VoigtFit could not retrieve a consistent fit for these galaxies.

abundance ratios in the diffuse gas. Relatively pristine gas would indicate an origin outside the galaxy, such as recent accretion, whereas enrichment with heavier elements would suggest material ejected from the galaxy by galactic winds.

The HI column densities for each source can be found in Table II. The transitions identified for both MW and galaxy components, continuum normalization fitting regions, and masks used are all listed in this online spreadsheet. The plots that are referred to for each galaxy can be found in the Appendix.

A. J0127-0619

In the galaxy J0127-0619 at z = 0.0054, we see blended Lyα troughs of the MW H I and source's component with a small peak due to their slight separation. We also observe a strong NV region from 1230.0 to 1257.0 Å which masks out almost the entire red wing of the Lyα trough. We ran only an unextended mask for both fixed and free fits, where the MW H I component is fixed to $\log[N(\mathrm{HI})] = 20.612$ cm^{-2} according to the Hartmann Atlas [4]. We see the unextended mask resulting in a MW H I column density of $\log[N(\mathrm{HI})] = 20.831 \pm 0.017$ cm^{-2} that overestimates and does not agree with the Hartmann Atlas value. Using the unextended mask, we obtained the galaxy HI component $\log[N(\mathrm{HI})] = 21.311 \pm 0.009$ and 21.210 ± 0.011 from the fixed and free fits respectively. The galaxy HI column density for the fixed fit is greater than the column density calculated in the free fit.

The MW metal lines that blend with DLA trough are: Si II 1190.4 and 1193.3; N I 1199.550049, 1200.2, and 1200.7; and Si III 1206.5. The galaxy metal lines that blend with the trough are Si II 1190.4 and 1193.3; N I 1199.6, 1200.2, and 1200.7 . The velocity offsets for S II and SiII was fixed for both components and N I's velocity offset for the MW component was fixed. We fixed the b-parameters of both the Si II and Si III ions for the MW component. These constraints were crated because of blending between galaxy and MW lines within the blending overtop the blue wing. MW N I lines blend with galaxy Si II 1193.3 and galaxy N I lines blend with MW Si III 1206.5.

When observing the subtracted fit graphs we see an

artifact around 1000 km km s^{-1} where we see a large emission peak followed by the masked NV region. The blue wing appears to be underfit, with the red continuum level not following through the center of the data across both fits. It is difficult to assess the value of this multi-absorption line fit for this galaxy due to the extreme NV region that could contain hidden Lyα emission.

B. J0144+0453

In the galaxy J0144+0453 at z = 0.0052, we see blended Lyα troughs of the MW H I and source's component with a small peak due to their slight separation. We also observe a weak NV region from 1236.20 to 1249.76 Å which does not greatly affect the shape of the red wing of the Lyα trough. We ran both fixed and free fits where the MW H I component is fixed with log[N(HI)] = 20.540 cm^{-2} according to the Hartmann Atlas.

When MW H I log[N(HI)] was free, the Hartmann Atlas value was within the uncertainty for the calculated MW H I column densities for the 1500 km s^{-1} and 2000 km s^{-1} mask. We see the unextended mask resulting in a column density that does not agree (though not far off), with a MW H I log[N(HI)] = 20.508 ± 0.011 cm^{-2}. This suggests that the extended masks provide a better overall fit.

The MW metal lines that blend with DLA trough are: N I 1199.6, 1200.2, and 1200.71; and SiIII 1206.5. The galaxy metal lines that blend with the trough are Si II 1190.4 and 1193.3; N I 1199.6, 1200.2, and 1200.71; and SiIII 1206.5. The galaxy's SiIII velocity offset was fixed as well as its b parameter. We fixed the b-parameters of both the Si II and Si III ions for both components, as well as the velocity offset at 0 (at source's rest wavelength) for the source's Si III component. This was done because VoigtFit consistently ignored fitting Si III and Si II when left with free parameters.

With fixed MW H I, we obtained source HI component with log[N(HI)] = 20.316 ± 0.008, 20.069 ± 0.024, 20.062± 0.027 cm^{-2} with Lyα masks unextended, extended to 1500 km s^{-1}, and extended to 2000 km s^{-2} respectively. For both 1500 km s^{-1} and 2000 km s^{-1} mask, the source's column densities agree within their uncertainties, whereas the unextended mask obtained a larger column density of log[N(HI)] = 20.316 ± 0.008.

When observing the subtracted fit graphs we see an artifact around 700 km km s^{-1} that looks like a small emission peak followed by a strong absorption feature. We also notice under fitting of data near the top of red wing at 2000 to 4000 km s^{-1} across all masked fits. In contrast, the blue damping wing appears to be more accurately constrained with all the metal and galaxy absorption lines fitted.

C. J0337-0502

In the galaxy J0337-0502 at z = 0.01352, this spectrum has less noise than other spectra. We see semi-blended Lyα troughs of the MW H I and source's component with no apparent Lyα emission, where the MW Lyα is in a detector gap. The fits all show a small peak between the troughs due to their slight separation. We do not observe an NV region in this spectrum. We ran only a fixed fit where the MW H I component's column density is log[N(HI)] = 20.566 cm^{-2} according to the Hartmann Atlas.

The MW metal lines that blend with DLA wings are: Si II 1190.415771 and 1193.289673; N I 1199.6, 1200.2, and 1200.71; SiIII 1206.5; and S II 1250.6, 1253.8, and 1259.5. The galaxy metal lines that are visible and blend with the trough are Si II 1190.4, 1193.3, and 1260.4; and S II 1250.6, 1253.8, and 1259.5. We fixed the MW S II velocity offset as well as the b-parameters of Si III for the MW component.

With fixed MW H I, we obtained source HI component with log[N(HI)] = 21.899 ± 0.002, 21.909 ± 0.002, 21.908 ± 0.002 cm^{-2} with Lyα masks unextended, extended to 1500 km s^{-1}, and extended to 2000 km s^{-2} respectively. For both 1500 km s^{-1} and 2000 km s^{-1} mask, the source's column densities agree within their uncertainties, whereas the unextended mask does not agree within the uncertainty but is 0.006 cm^{-2} off.

When observing the subtracted fit graphs, we observe that at the end of both the blue and red wing we under fit with the new continuum level. We see a symmetry of two peaks, which suggests that VoigtFit did not estimate the column density of the galaxy's H I correctly. Whereas in the blue wing we see the red continuum level pass through the center of the black spectral data specifically around the metal lines which can also be seen in the red wing. Towards the bottoms of the wings at -3000 km s^{-1} and +3000 km s^{-1} is where we see this under fitting and these two emission peak artifacts.

D. J0405-3648

In the galaxy J0405-3648 at z = 0.002800, we see a narrow blended trough of the MW H I and source's component. We also observe a weak NV region from 1237.14 to 1248.56 Å which does not greatly affect the shape of the red wing of the Lyα trough, or blend with other metal lines. We only ran a fit with free MW H I column density since we were unable to retrieve the MW H I column density from Hartmann Atlas. We obtained MW H I component with log[N(HI)] = 20.376 ± 0.025, 19.210 ± 0.183, 18.821± 0.576 cm^{-2} with Lyα masks unextended, extended to 1500 km s^{-1}, and extended to 2000 km s^{-2} respectively. These larger uncertainties for the extended masks' column densities suggest that the extended masks are not reliable for this spectrum.

The MW metal lines that blend with DLA wings are: Si II 1190.4 and 1193.289673; N I 1199.6, 1200.2, and 1200.71; SiIII 1206.5. The galaxy metal lines that are visible and blend with the trough are Si II 1190.4 and 1193.3; N I 1199.6, 1200.2, and 1200.71; and SiIII 1206.5. We fixed the MW S II velocity offset as well as the b-parameters of Si III for the MW component.

We obtained the source HI component with log[N(HI)] = 20.854 ± 0.008, 21.010 ± 0.007, 21.042± 0.008 cm^{-2} with Lyα masks unextended, extended to 1500 km s^{-1}, and extended to 2000 km s^{-2} respectively. These values do not agree either.

When observing the subtracted fit graphs, we observe that the region at -1000 to -2000 km s^{-1} is severely underfit at different levels for different masks. For the 1500 km s^{-1} mask, the best fit line seems to fit the best here, however this fit is still not great. This area could be potential emission from the galaxy blended with the geocoronal emission at MW H I. We also see the bottom of the blue wing being underfit with artifacts in the subtracted graph as a broad emission profile from 700 to 2000 km s^{-1}.

E. J0934+5514

For the galaxy J0934+5514 at z = 0.0025, we have a less noisy spectrum. We observe a blended trough of the MW H I and source's component with no apparent Lyα emission. We also observe a weak NV region from 1237.41 to 1247.0 Å which does not greatly affect the shape of the red wing of the Lyα trough, or blend with S II metal lines. We ran only a fixed fit where the MW H I component's column density is log[N(HI)] = 20.408 cm^{-2} according to the Hartmann Atlas.

The MW metal lines that blend with DLA wings are: Si II 1190.4, 1193.3, and 1260.4; N I 1199.6, 1200.2, and 1200.71; SiIII 1206.5; and S II 1250.6, 1253.8, and 1259.5. The galaxy metal lines that are visible and blend with the trough are Si II 1190.4, 1193.3, and 1260.4; N I 1199.6, 1200.2, and 1200.71; SiIII 1206.5; and S II 1250.6, 1253.8, and 1259.5. For both components, we fixed the velocity offset of the Fe II and CII* transitions. For solely MW metal lines, we fixed only PII, and the galaxy metal lines we fixed NI. We also fixed the b-parameters if the SiII and SiIII ions for both components.

With fixed MW H I, we obtained source HI component with log[N(HI)] = 21.314 ± 0.001, 21.323 ± 0.001, 21.331 ± 0.001 cm^{-2} with Lyα masks unextended, extended to 1500 km s^{-1}, and extended to 2000 km s^{-2} respectively. While the column densities from 1500 km s^{-1} and 2000 km s^{-1} mask do not agree within their uncertainties, they are in a similar range. Once again, we see the unextended mask does not agree with either of the extended masks' column densities.

When observing the subtracted fit graphs, we observe that both the blue and red wings seem to subtract nicely to 0. The bottom of the blue wing goes down to 0. However, we see on the bottom of the red wing from 1000 to 1750 km s^{-1} a broad emission feature similar to other spectra. This may be real Lyα emission, or it could be an artifact from under fitting as we suspect from other examples.

F. J0940+2935

The galaxy J0940+2935 at z = 0.001675 is the lowest redshift of our subset of DLAs. We observe blending of the MW H I trough and the source's HI trough. There may be a slight Lyα emission at 320 km s^{-1}. This galaxy also has a weak NV region spanning from 1237.08 to 1247.18 Å which falls towards the right end of the red damping wing of the Lyα trough. We ran both fixed and free MW H I fits where fixed MW H I log[N(HI)] = 20.231 cm^{-2}. We obtained MW H I component with log[N(HI)] = 20.845 ± 0.032, 20.663 ± 0.053, 20.266± 0.131 cm^{-2} with Lyα masks unextended, extended to 1500 km s^{-1}, and extended to 2000 km s^{-2} respectively.

The MW metal lines that blend with DLA wings are: Si II 1190.4, 1193.3, and 1260.4; N I 1199.6, 1200.2, and 1200.71; SiIII 1206.5; and S II 1250.6, 1253.8, and 1259.5. The galaxy metal lines that are visible and blend with the trough are Si II 1190.4, 1193.3, and 1260.4; N I 1199.6, 1200.2, and 1200.71; SiIII 1206.5; and S II 1250.6, 1253.8, and 1259.5. Many ions had fixed velocity components due to VoigtFit unable to fit the data for this galaxy with velocity offsets left free. For the Milky Way component, this includes: Fe II, N I, S II, O I, C II, and CII *. For the galaxy component this includes: Fe II, N I, C II, and C II*. The b-parameter for the Si II and Si II ions were fixed for both components.

For fixed MW H I, we obtained source column densities that do not agree at log[N(HI)] = 21.363 ± 0.004, 21.375 ± 0.004, 21.393 ± 0.004 cm^{-2} with Lyα masks unextended, extended to 1500 km s^{-1}, and extended to 2000 km s^{-2} respectively.

For free MW H I, we obtained source column densities that do not agree at log[N(HI)] = 21.265 ± 0.013, 21.322 ± 0.012, 21.392 ± 0.011 cm^{-2} with Lyα masks unextended, extended to 1500 km s^{-1}, and extended to 2000 km s^{-2} respectively. For the free MW H I fits, there is a large range in column densities than the fixed MW H I fits. Another observation is that the column densities for the 2000 km s^{-2} mask agree within their uncertainties for both fixed and free fits.

However, in all subtracted fit plots we do see the bottom of the trough slightly above zero, and once again beginning at 2000 km s^{-1} we see a broad emission feature across all masks which is most likely due to under fitting of the bottom of the red wing. We also notice under fitting of data near the top of red wing at 2000 to 4000 km s^{-1} across all masked fits. From -1300 to -2000 km s^{-1}in the blue wing, we also see a broad emission

feature which can be due to under-fitting.

G. J1044+0353

In the spectrum for galaxy J1044+0353 at z = 0.012870, we observe blending of the MW H I trough and the source's HI trough with visible Lyα emission. There is a weak NV region from 1244.3 to 1253.0 Å in the red damping wing of the Lyα trough. Therefore, we ran a fit with a fixed MW H I at log[N(HI)] = 20.576 cm^{-2} according to the Hartmann Atlas [4]. We ran both fixed and free MW H I fits where fixed MW H I at log[N(HI)] = 20.576 cm^{-2}. We obtained free MW H I component with log[N(HI)] = 20.401 ± 0.025, 20.495 ± 0.021, 20.591 ± 0.019 cm^{-2} with Lyα masks unextended, extended to 1500 km s^{-1}, and extended to 2000 km s^{-2} respectively. The extended 2000 km s^{-1} mask agrees with Hartman Atlas value within its uncertainty, but the other calculated column densities do not agree and are less than Hartman Atlas value.

The MW metal lines that blend with DLA wings are: Si II 1190.4, 1193.3, and 1260.4; N I 1199.6, 1200.2, and 1200.71; SiIII 1206.5; and S II 1250.6, 1253.8, and 1259.5. The galaxy metal lines that are visible and blend with the trough are Si II 1190.4, 1193.3, and 1260.4; N I 1199.6, 1200.2, and 1200.71; SiIII 1206.5; and S II 1250.6, 1253.8, and 1259.5. For the Milky Way component, we fixedthe velocity offset at 0 (at Milky Way's rest wavelength) for SII and CII* 1335 ions; for the galaxy's components, we fixed the velocity offset for CII* 1335 ion. We fixed the b-parameters of both the Si II and Si III ions for both components.

For fixed MW H I, we obtained source H I column densities at log[N(HI)] = 21.879 ± 0.005, 21.855 ± 0.004, 21.858± 0.004 cm^{-2} with Lyα masks unextended, extended to 1500 km s^{-1}, and extended to 2000 km s^{-2} respectively. For both the 1500 and 2000 km s^{-1} mask, the source column densities agree within their uncertainties, but the unextended mask does not. For free MW H I, we obtained source column densities at log[N(HI)] = 21.907 ± 0.005, 21.871 ± 0.005, 21.849 ± 0.005 cm^{-2} with Lyα masks unextended, extended to 1500 km s^{-1}, and extended to 2000 km s^{-1} respectively. None of these source column densities agreed within their uncertainties. However, the 2000 km s^{-1} mask agrees within the uncertainties for both the free and fixed fits.

In all subtracted fit plots, the bottom of the trough is above the zero line which suggests the need to account for partial covering. We observe two broad emission features opposite of the Lyα emission at the bottom of the red wing from 1500 to 3400 km s^{-1} and at -3200 to -1600 km s^{-1} which may be due to under fitting. However these broad emission features are asymmetric, suggesting this shape is dependent on another factor. The majority of the blue damping wing appears to be accurately constrained through all fits.

H. J1105+4444

For the galaxy J1105+4444 at z = 0.02154, we observe semi-blended Lyα troughs of the MW H I and source's component with visible Lyα emission at 510 km s^{-1} , where the MW Lyα absorption is in a detector gap. We observe a strong NV region from 1256.0 to1276.0 Å in this spectrum. We ran only a fixed fit where the MW H I component's column density is log[N(HI)] = 20.566 cm^{-2} according to the Hartmann Atlas.

The MW metal lines that are visible and blend with DLA wings are: Si II 1190.415771 and 1193.289673; N I 1199.6, 1200.2, and 1200.71; and SiIII 1206.5. There is no MW S II component that is fixed because these transitions overlap with the masked NV region. The galaxy metal lines that are visible and blend with the trough are Si II 1190.4, 1193.3, and 1260.4; and S II 1250.6, 1253.8, and 1259.5. We fixed the MW S II velocity offset as well as the b-parameters of Si III for the MW component.

With fixed MW H I, we obtained source HI component with log[N(HI)] = 21.478 ± 0.004, 21.488 ± 0.004, 21.508 ± 0.005 cm^{-2} with Lyα masks unextended, extended to 1500 km s^{-1}, and extended to 2000 km s^{-1} respectively. For both unextended and 1500 km s^{-1}, the source's column densities fall close within their uncertainties at 0.002 off, whereas the 2000 km s^{-1} mask does not agree within the uncertainties as well but is farther off from the other column densities.

When observing the subtracted fit graphs, we observe that at the end of both the blue and red wing we under fit with the new continuum level. In the red wing from 850 to 3400 km s^{-1}, we see the red best fit line severely underfit this area which results in a broad emission feature. We also see the regions around the detector gap rise higher above 0, pointing to under-fitting of the supposed MW H I trough that we fit, suggesting that this fixed MW H I model is inaccurate in the shape of its wings.

I. J1129+2034

The galaxy J1129+2034 at z = 0.004703, we observe blending of the MW H I trough and the source's HI trough with no apparent Lyα emission. This galaxy also has a strong NV region spanning from 1233.6 to 1252.5 Å which falls towards the right end of the red damping wing. We ran both fixed and free MW H I fits where fixed MW H I log[N(HI)] = 20.175 cm^{-2}. We obtained MW H I component with log[N(HI)] = 19.984 ± 0.032, 19.848 ± 0.041, 19.593± 0.068 cm^{-2} with Lyα masks unextended, extended to 1500 km s^{-1}, and extended to 2000 km s^{-2} respectively. These MW H I column densities are much lower than the Hartmann Atlas column density.

The MW metal lines that blend with DLA wings are: Si II 1190.4, 1193.3, and 1260.4; N I 1199.6, 1200.2, and 1200.71; SiIII 1206.5; and S II 1250.6, 1253.8, and 1259.5. The galaxy metal lines that are visible and blend with the

trough are Si II 1190.4, 1193.3, and 1260.4; N I 1199.6, 1200.2, and 1200.71; SiIII 1206.5; and S II 1250.6, 1253.8, and 1259.5. For the Milky Way component, we fixed velocity offset of S II; and for the galaxy component we fixed velocity offset of Si III. We also fixed b-parameters of Si II and Si III ions for both components.

For fixed MW H I, we obtained source column densities that do not agree at $\log[N(\mathrm{HI})] = 21.233 \pm 0.005$, 21.249 ± 0.005, 21.275 ± 0.005 cm^{-2} with Lyα masks unextended, extended to 1500 km s^{-1}, and extended to 2000 km s^{-2} respectively. For free MW H I, we obtained source column densities that do not agree at $\log[N(\mathrm{HI})] = 21.265 \pm 0.013$, 21.322 ± 0.012, 21.392 ± 0.011 cm^{-2} with Lyα masks unextended, extended to 1500 km s^{-1}, and extended to 2000 km s^{-2} respectively. Overall, the free fits with MW H I column densities in the 19 cm^{-2} range results in higher calculated galaxy H I column densities for each type of mask, compared to the fixed fit galaxy column densities.

In all subtracted fit plots, we see the bottom of the trough at zero. In the fixed fits, we see the continuum level pass through the spectral data better than the free fits in the region after the Si III 1206 absorption line (in the blue wing). Once again at 1000 to 2500km s^{-1}, we see a broad emission feature across all masks which is most likely due to under fitting of the bottom of the red wing, we have seen in other spectra. Most of the spectral data in the subtracted fits tends to be centered closer to 0 despite these previous observations, meaning that the best fit line more accurately represents the absorption features in this spectra.

J. J1132+1411

The galaxy J1132+1411 at z = 0.017637, we observe separated MW H I trough and source's H I trough with no visible Lyα emission from the source. This galaxy also has a strong NV region spanning from 1245.8 to 1271.2 Å which falls towards the right end of the red damping wing of the galaxy trough. We ran both fixed and free MW H I fits where fixed MW H I $\log[N(\mathrm{HI})] = 20.537$ cm^{-2}. We obtained MW H I component with $\log[N(\mathrm{HI})] = 20.683 \pm 0.013$, 20.616 ± 0.015, 20.618 ± 0.014 cm^{-2} with Lyα masks unextended, extended to 1500 km s^{-1}, and extended to 2000 km s^{-2} respectively. These MW H I column densities are all higher than the Hartmann Atlas column density. Because of the trough separation, there are no MW metal lines that blend with the galaxy's DLA wings. The galaxy metal lines that are visible and blend with the trough are SiIII 1206.5.

For fixed MW H I, we obtained source H I column densities at $\log[N(\mathrm{HI})] = 20.688 \pm 0.009$, 20.714 ± 0.011, 20.722 ± 0.013 cm^{-2} with Lyα masks unextended, extended to 1500 km s^{-1}, and extended to 2000 km s^{-2} respectively. For both 1500 km s^{-1} and 2000 km s^{-1} mask, the source's column densities agree within their uncertainties, whereas the unextended mask does not agree within the uncertainty at a much lower value. For free MW H I, we obtained source column densities that all agree within their uncertainties at $\log[N(\mathrm{HI})] = 20.662 \pm 0.010$, 20.678 ± 0.012, 20.674 ± 0.011 cm^{-2} with Lyα masks unextended, extended to 1500 km s^{-1}, and extended to 2000 km s^{-1} respectively. Overall, the fixed fits resulted in higher calculated galaxy H I column densities for each type of mask, compared to the free fit galaxy column densities.

In all subtracted fit plots, we see the bottom of the source's trough centered at zero. However, the bottom of the red wing and blue wing are under-fitted as seen by the two emission features at both -1000 to -400 km s^{-1} and 320 to 1000 km s^{-1}. We also see the region between the two troughs from -3400 to -1800 km s^{-1} over-fitted.

K. J1150+1501

The galaxy J1150+1501 at z = 0.002448, we observe blending of the MW H I trough and the source's HI trough with no apparent Lyα emission. This galaxy also has a strong NV region spanning from 1231.5 to 1248.3 Å which falls towards the right end of the red damping wing. We ran both fixed and free MW H I fits where fixed MW H I $\log[N(\mathrm{HI})] = 20.523$ cm^{-2}. We obtained MW H I component with $\log[N(\mathrm{HI})] = 21.018 \pm 0.014$, 20.622 ± 0.021, 20.518 ± 0.036 cm^{-2} with Lyα masks unextended, extended to 1500 km s^{-1}, and extended to 2000 km s^{-2} respectively. The extended 2000 km s^{-2} mask's column density agrees with Hartmann Atlas value, while both extended 1500 km s^{-2} and unextended mask's column densities are greater than the Hartman Atlas value.

The MW metal lines that blend with DLA wings are: Si II 1190.4, 1193.3, and 1260.4; N I 1199.6, 1200.2, and 1200.71; and SiIII 1206.5. The galaxy metal lines that are visible and blend with the trough are Si II 1190.4, 1193.3, and 1260.4; N I 1199.6, 1200.2, and 1200.71; and SiIII 1206.5. For the Milky Way component, we fixed the velocity offset of C II, C II*, and Si IV; for the galaxy's component, we fixed the velocity offset of the P II, S II, and O I ions. We fixed the b-parameters of both the Si II and Si III ions for both components. The Si III 1206 absorption feature was modeled in all fits except for the free MW H I, unextended mask fit which could explain the discrepancy between unextended, free mask MW H I column density and other column densities mentioned previously.

For fixed MW H I, we obtained source H I column densities at $\log[N(\mathrm{HI})] = 21.086 \pm 0.004$, 21.111 ± 0.005, 21.138 ± 0.005 cm^{-2} with Lyα masks unextended, extended to 1500 km s^{-1}, and extended to 2000 km s^{-2} respectively. These source's column densities do not agree within their uncertainties. For free MW H I, we obtained source column densities that all agree within their uncertainties at $\log[N(\mathrm{HI})] = 20.886 \pm 0.013$, 21.082 ± 0.008, 21.151 ± 0.008 cm^{-2} with Lyα masks unextended, extended to 1500 km s^{-1}, and extended to 2000 km s^{-1}

respectively. Both unextedned and 1500 km s^{-1}, resulted in lower source column densities, whereas the 2000 km s^{-1} mask resulted in slightly higher column density than the fixed fit calculated, which follows the idea that the MW H I column density was slightly less than the Hartmann value.

In all subtracted fit plots, we see the bottom of the trough lie above the zero line suggesting partial covering of H I at play for this spectra. Except for the free and unextended mask fit, the bottom of the blue wing is centered at 0 which suggests the blue wing is well constrained. Once again, we see this residual emission feature from 500 to 1300 km s^{-1} in the bottom of the red wing.

L. J1225+6109

The galaxy J1225+6109 at z = 0.002341, we observe blending of the MW H I trough and the source's HI trough with no apparent Lyα emission. This galaxy also has a strong NV region spanning from 1231.1 to 1248.3 Å which falls towards the right end of the red damping wing. We ran both fixed and free MW H I fits where fixed MW H I log[N(HI)] = 20.187 cm^{-2}. We obtained free MW H I component with log[N(HI)] = 20.620 ± 0.029, 20.452 ± 0.046, 20.143 ± 0.096 cm^{-2} with Lyα masks unextended, extended to 1500 km s^{-1}, and extended to 2000 km s^{-2} respectively. The extended 2000 km s^{-2} mask's column density agrees with Hartmann Atlas value, while both extended 1500 km s^{-2} and unextended mask's column densities are greater than the Hartman Atlas value.

The MW metal lines that blend with DLA wings are: Si II 1190.4, 1193.3, and 1260.4; N I 1199.6, 1200.2, and 1200.71; SiIII 1206.5; and S II 1250.6, 1253.8, and 1259.5. The galaxy metal lines that are visible and blend with the trough are Si II 1190.4, 1193.3, and 1260.4; N I 1199.6, 1200.2, and 1200.71; SiIII 1206.5; and S II 1250.6, 1253.8, and 1259.5. For the Milky Way components, we fixed the velocity offset of all ions at ranges from -730 to -760 km s^{-1}; for the galaxy's components, we fixed the velocity offset of all ions in the range 10 to 40 km s^{-1}. We fixed the b-parameters of both the Si II and Si III ions for both components.

For fixed MW H I, we obtained source H I column densities at log[N(HI)] = 21.378 ± 0.004, 21.384 ± 0.004, 21.400 ± 0.005 cm^{-2} with Lyα masks unextended, extended to 1500 km s^{-1}, and extended to 2000 km s^{-2} respectively. These source's column densities do not agree within their uncertainties. For free MW H I, we obtained source column densities that do not agree within their uncertainties at log[N(HI)] = 21.339 ± 0.010, 21.359 ± 0.008, 21.405 ± 0.008 cm^{-2} with Lyα masks unextended, extended to 1500 km s^{-1}, and extended to 2000 km s^{-1} respectively. Both unextended and 1500 km s^{-1} in the free fits, resulted in lower source column densities than their fixed fits counterparts. However, the 2000 km s^{-1} mask resulted in a source column density which agrees within the uncertainty of the same mask, fixed fit calculated source column density.

In all subtracted fit plots, we see the bottom of the trough lie above the zero line suggesting partial covering of H I at play for this spectra. We also observe that at the end of both the blue and red wing we under fit with the new continuum level, but the broad emission features known to appear from this under-fitting are not symmetric. In the blue wing from -2000 to -1300 km s^{-1}, we see the spectral data rise higher than the region in the red wing from 900 to 2000 km s^{-1}.

M. J1359+5726

The galaxy J1359+5726 at z = 0.033829 is the highest redshift galaxy in our DLA subset. We observe separation of the MW H I trough and the source's HI trough with extreme Lyα emission comparable to the scale of geocoronal emission on the spectrum. This galaxy also has a weak NV region spanning from 1271.9 to 1287.8 Å which falls towards the right end of the red damping wing. We ran both fixed and free MW H I fits where fixed MW H I log[N(HI)] = 20.138 cm^{-2}. We obtained free MW H I component with log[N(HI)] = 20.118 ± 0.012, 20.124 ± 0.007, 20.121 ± 0.012 cm^{-2} with Lyα masks unextended, extended to 1500 km s^{-1}, and extended to 2000 km s^{-2} respectively. All free fit MW H I column densities are less than Hartmann Atlas value, and none of these values agree within their uncertainties. However, these Mw H I column densities fall within a similar range at most 0.008 cm^{-2} off from agreeing within uncertainties.

The MW metal lines that blend with DLA wings are: NV 1238 and 1242; Si II 1260.4; and S II 1250.6, 1253.8, and 1259.5. The galaxy metal lines that are visible and blend with the trough are Si II 1190.4 and 1193.3; N I 1199.6, 1200.2, and 1200.71; and SiIII 1206.5. For the Milky Way component, we fixed the velocity offset of S II, and we fixed the b-parameters of both the Si II and Si III ions.

For fixed MW H I, we obtained source H I column densities at log[N(HI)] = 20.719 ± 0.008, 20.800 ± 0.008, 20.816 ± 0.009 cm^{-2} with Lyα masks unextended, extended to 1500 km s^{-1}, and extended to 2000 km s^{-2} respectively. For the 1500 and 2000 km s^{-1} mask, the source H I column densities agree within their uncertainties, but the unextended mask does not agree with any other mask. For free MW H I, we obtained source column densities that do not agree within their uncertainties at log[N(HI)] = 20.734 ± 0.008, 20.790 ± 0.008, 20.850 ± 0.007 cm^{-2} with Lyα masks unextended, extended to 1500 km s^{-1}, and extended to 2000 km s^{-1} respectively. None of these source column densities agree within their uncertainties. However the unextended and 1500 km s^{-1} mask agree within the uncertainties of their fixed fit counterparts.

In all subtracted fit plots, the bottom of the trough lies above the zero line from -1200 to 1500 km s^{-1} which suggests the need to account for partial covering of H I for this spectrum. We observe that at the end of both the blue and red wing we severely under fit with the new continuum level, which can be attributed to not accounting for partial covering. We also see over-fitting of spectral data from 1500 to 3500 km s^{-1} in the red wing. There is more work to be done with constraining the metal lines blended with the blue wing as well.

N. J1444+4237

In the spectra for galaxy J1444+4237 at z = 0.002300, we observe blending of the MW H I trough and the source's HI trough with no apparent Lyα emission. This galaxy also has a weak NV region spanning from 1239.0 to 1248.1 Å which falls towards the right end of the red damping wing. We ran both fixed and free MW H I fits where fixed MW H I log[N(HI)] = 20.109 cm^{-2}. We obtained free MW H I component with log[N(HI)] = 20.494 ± 0.046, 20.184 ± 0.141, 20.208 ± 0.175 cm^{-2} with Lyα masks unextended, extended to 1500 km s^{-1}, and extended to 2000 km s^{-2} respectively. All MW H I column densities are greater than Hartmann Atlas value, and only 1500 and 2000 km s^{-1} mask agree within their large uncertainties.

The MW metal lines that blend with DLA wings are: Si II 1190.4, 1193.3, and 1260.4; N I 1199.6, 1200.2, and 1200.71; Si III 1206.5; and S II 1250.6, 1253.8, and 1259.5. The galaxy metal lines that are visible and blend with the trough are Si II 1190.4, 1193.3, and 1260.4; N I 1199.6, 1200.2, and 1200.71; Si III 1206.5; and S II 1250.6, 1253.8, and 1259.5. For the Milky Way components, we fixed the velocity offset of all ions at ranges from -742 to -712 km s^{-1}; for the galaxy's components, we fixed the velocity offset of all ions in the range -90 to -30 km s^{-1}. We fixed the b-parameters of both the Si II and Si III ions for both components.

For fixed MW H I, we obtained source H I column densities at log[N(HI)] = 21.598 ± 0.003, 21.598 ± 0.003, 21.599 ± 0.003 cm^{-2} with Lyα masks unextended, extended to 1500 km s^{-1}, and extended to 2000 km s^{-2} respectively. All these source H I column densities agree within their uncertainties. For free MW H I, we obtained source column densities at log[N(HI)] = 21.596 ± 0.009, 21.597 ± 0.007, 21.597 ± 0.008 cm^{-2} with Lyα masks unextended, extended to 1500 km s^{-1}, and extended to 2000 km s^{-1} respectively. All of these source H I column densities agree within their uncertainties. Furthermore, both fixed and free fits for every mask resulted in source H I column densities that agreed within their uncertainties which suggests little effect using these different masks.

In all subtracted fit plots, the bottom of the trough is centered at zero line. We observe that at the end of both the blue and red wing we slightly under fit with the red line, however this is also close to centered at zero which suggests that both wings are well-constrained in comparison to previous spectra. From 1800 to 3100 km s^{-1} in the red wing, we observe a slight broad emission feature with spectral data above zero. While there is no Lyα emission profile to retrieve, we can be confident this spectrum is well constrained by our defined absorption features because of this subtracted fit with spectral data centered at 0.

O. J1448-0110

For the galaxy J1448-0110 at z = 0.027412, we observe semi-blended, but separated Lyα troughs of the MW H I and source's component with no apparent Lyα emission, where the MW Lyα absorption is in a detector gap. We observe a strong NV region from 1264.0 to 1280.7 Å in this spectrum. We ran only a fixed fit where the MW H I component's column density is log[N(HI)] = 20.589 cm^{-2} according to the Hartmann Atlas.

The MW metal lines that blend with DLA wings are: Si II 1190.4, 1193.3, and 1260.4; N I 1199.6, 1200.2, and 1200.71; SiIII 1206.5; and S II 1250.6, 1253.8, and 1259.5. The galaxy metal lines that are visible and blend with the trough are P II 1152, Si II 1190.4, 1193.3, and 1260.4; N I 1199.6, 1200.2, and 1200.71; SiIII 1206.5; and S II 1250.6, 1253.8, and 1259.5. For the MW component, we fixed the velocity offset of Si III; for the galaxy component, we fixed Si III ion entirely at log[N(HI)] = 14.5 cm^{-2}.

With fixed MW H I, we obtained source HI component with log[N(HI)] = 21.614 ± 0.004, 21.617 ± 0.004, 21.623 ± 0.004 cm^{-2} with Lyα masks unextended, extended to 1500 km s^{-1}, and extended to 2000 km s^{-1} respectively. All calculated source column densities agree within their uncertainties which suggests little effect using these different masks.

In all subtracted fit plots, the bottom of the trough is centered at zero line. The blue wing appears well-constrained by the MW and galaxy metal lines. However, we observe that at the end of both the blue and red wing we under fit with the red line, which results in broad emission features at -2000 to 1350 km s^{-1} and 1200 to 2300 km s^{-1}. These emission features are not symmetric which suggests that these shapes are dependent on more than just under-fitting.

IV. CONCLUSION

For the sample of DLAs where we ran both fixed and free fits, we can estimate standard error for MW H I column density and galaxy H I column density for all unextended, extended 1500, and 2000 km s^{-1} masks. We use the sample mean ($\bar{x}$) of log[N(HI)] = 20.336 cm^{-2} from the Hartmann Atlas values with standard error ($\sigma_{\bar{x}}$) = 0.067. For free MW H I extended 1500 km s^{-1} mask,

we obtained $\bar{x} = 20.395$ cm^{-2} with $\sigma_{\bar{x}} = 0.094$ which is closest to the statistical error of the Hartman Atlas values which leads us to believe this is the best mask to use. $\sigma_{\bar{x}}$ ranges from 0.164 to 0.181 for the source column densities from both free and fixed MW H I fits.

Generally, it appears that the unextended mask does not obtain MW H I column densities that agree with the Hartman Atlas column density. This suggests that masking for residual Lyα emission is a more accurate representation of these spectra, since these masks obtained more consistent MW H I column densities within the statistical error.

In the subtracted fit plots, it was typical for the bottom of the red wing of the Lyα damped absorption to be under-fit which left a broad emission feature. This feature could be residual Lyα emission, however we believe this artifact could also be attributed to systematic error in the absorption line profile shape of the trough. For some spectra, there were symmetric blue wing and red wing under-fitting near the bottom of the trough which left asymmetric broad emission features opposite of both sides of the source's Lyα rest wavelength. Other than this under-fitting near the bottom, the blue wing with blended MW and galaxy metal lines seemed to be more accurately constrained throughout all spectra.

A few notable spectra are J1105+4444, J0337-0502, and J1448-0110 which contained a data gap over the region where the MW absorption trough would exist. For these galaxies, we only ran fixed fits. However in J1105+4444 and J0337-0502, the detector gap over MW H I resulted in troughs that would otherwise have been blended, appearing to have separation and less of an effect on the width of the blended trough. J1448-0110 contradicts this as it looks like it's modeled well with a fixed MW H I component especially on the right wing. It is worth considering running a fit where one does not define a MW H I component for J1105+4444 and J0337-0502 in order to examine if this fixed component leads to larger inaccuracies in the data.

Future work will involve using H I column densities to measure chemical abundances as well as radiative transfer modeling. If galaxies show $\Delta N(HI)_{MW} > 0.5$ dex in the free MW H I column densities from different masks, these fits are not accurate enough to model from. However, if the free extended masks agree with Hartmann Atlas value, this is worth modeling from. For example, the case of J0940+2935 where the 2000 km/s for MW H I component is within the dex of Hartman Atlas column density is worthwhile to analyze further.

For modeling Lyα emission there are a subset of this sample that have robust Lyα features and can possibly be modeled J1225+6109, J1444+4237, and J1448-0110 have slight Lyα emission near the source's rest wavelength, however the trough is extremely saturated so it's unclear whether anything can be modeled from this. In contrast, the spectra J1044+0353, J0940+2935, J1129+2034, J1359+5726, and J1105+4444 have extreme visible Lyα emission near the bottom of the trough. J1105+4444 blends with the right wing, so the under-fitting of this red wing issue that occurs through all subtracted fits will prove detrimental to modeling the line profile using the subtracted fit.

ACKNOWLEDGMENTS

I wish to acknowledge the support of my faculty advisor, Dr. Crystal Martin who I worked closely with throughout this research project. Thank you to the REU site director, Dr. Sathya Guruswamy, who guided me through the research process as well as coordinating professional development activities. I also would like to thank Nimisha Kumari for providing the foundation for the python programs, as well as beneficial discussion on the line-fitting process, and Xinfeng Xu for providing the extended source line-spread function tables for our sample. I also would like to thank the National Science Foundation Grant PHY-1852574 that allowed this research to be possible. Lastly, I want to thank my family for their support and encouragement through this milestone in my academic career.

[1] N. S. Foundation, First stars and first light: Epoch of reionization, Available at `https://www.nsf.gov/news/special_reports/astronomy/epoch_reionization.pdf` (2021/07/30).

[2] B. L. James, A. Aloisi, T. Heckman, S. T. Sohn, and M. A. Wolfe, Investigating Nearby Star-forming Galaxies in the Ultraviolet with HST/COS Spectroscopy. I. Spectral Analysis and Interstellar Abundance Determinations, Astrophys. J. **795**, 109 (2014), arXiv:1408.4420 [astro-ph.GA].

[3] J.-K. Krogager, Voigtfit: A python package for voigt profile fitting (2018), arXiv:1803.01187 [astro-ph.IM].

[4] D. Hartmann and W. B. Burton, *Atlas of Galactic Neutral Hydrogen* (1997).

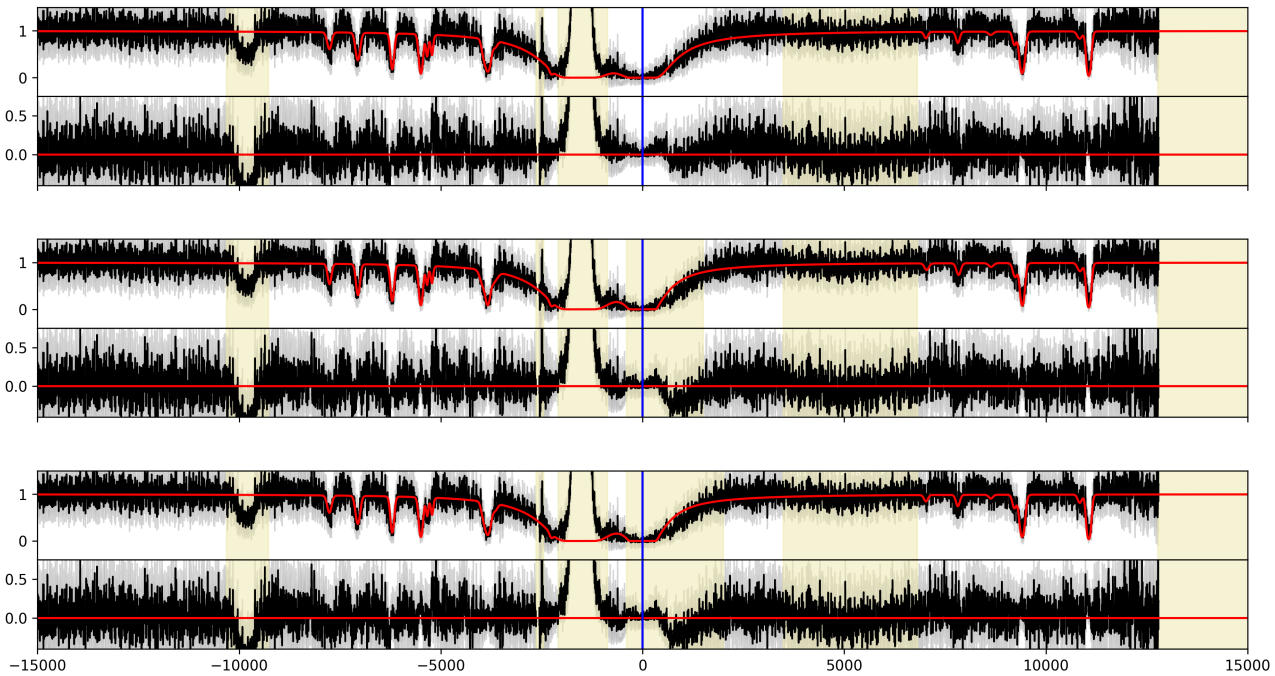

FIG. 3: Galaxy J0144+0453 with z = 0.0052 with fit using fixed MW H I component, with each figure from top to bottom showing a non-extended mask, extended mask to 1500 km s^{-1}, and extended mask to 2000 km s^{-1} respectively. In each figure, top plot shows absorption line fit (red), spectral data(black), and masks (yellow). Bottom plot shows the resulting Lyα emission profile with a subtracted absorption line fit(red), subtracted spectral data (black), and masks (yellow). Blue line in all plots is the source's Lyα rest wavelength.

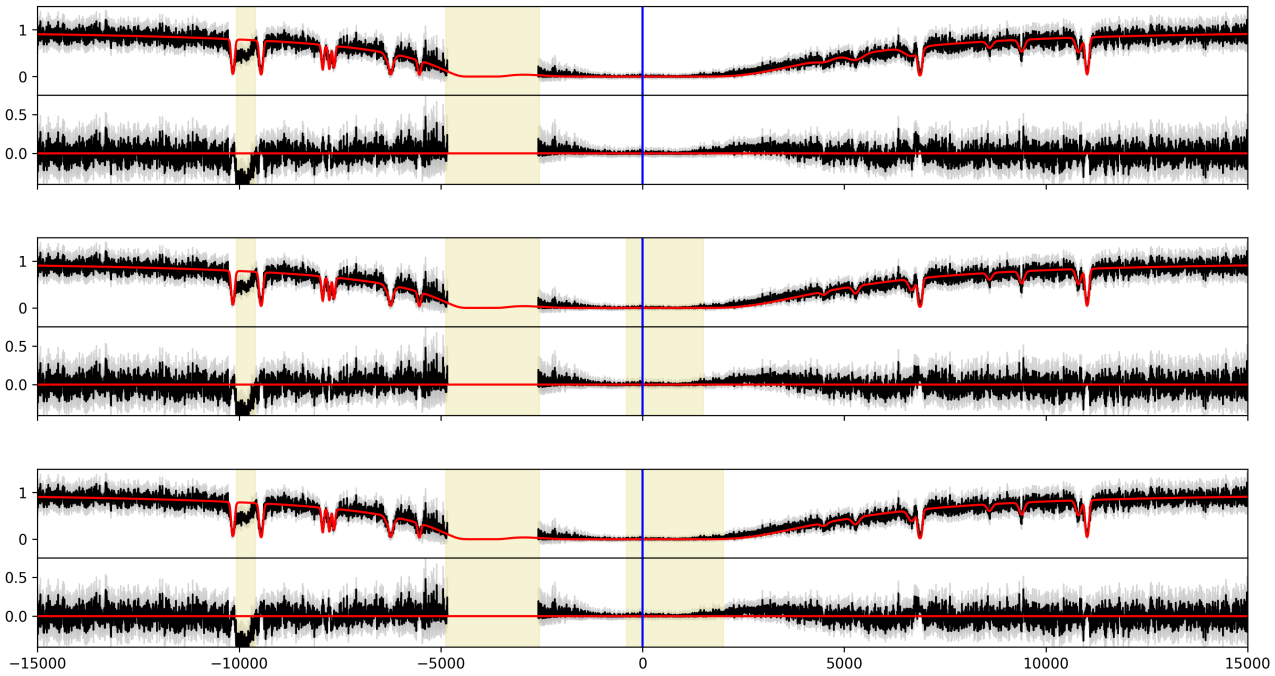

FIG. 4: Galaxy J0337-0502 with z = 0.01352 with fit using fixed MW H I component.

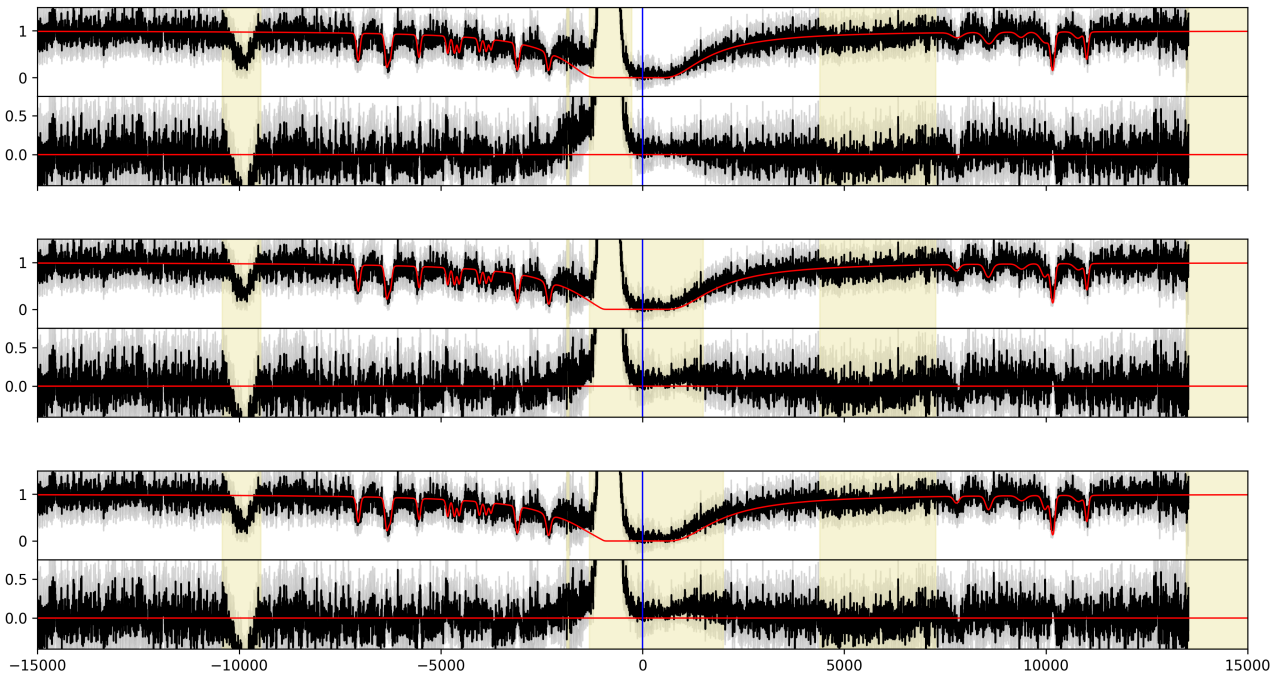

FIG. 5: Galaxy J0405-3648 with z = 0.0028 with fit using free MW H I component.

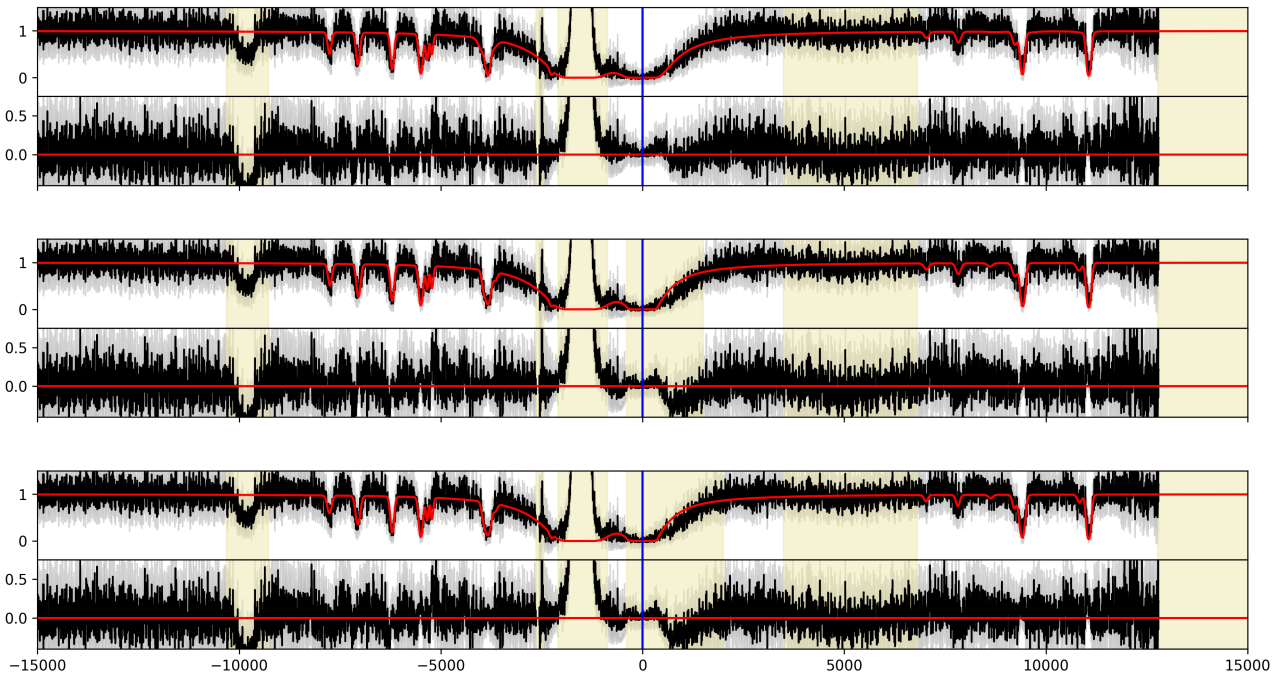

FIG. 6: Galaxy J0144+0453 with z = 0.0052 with fit using free MW H I component.

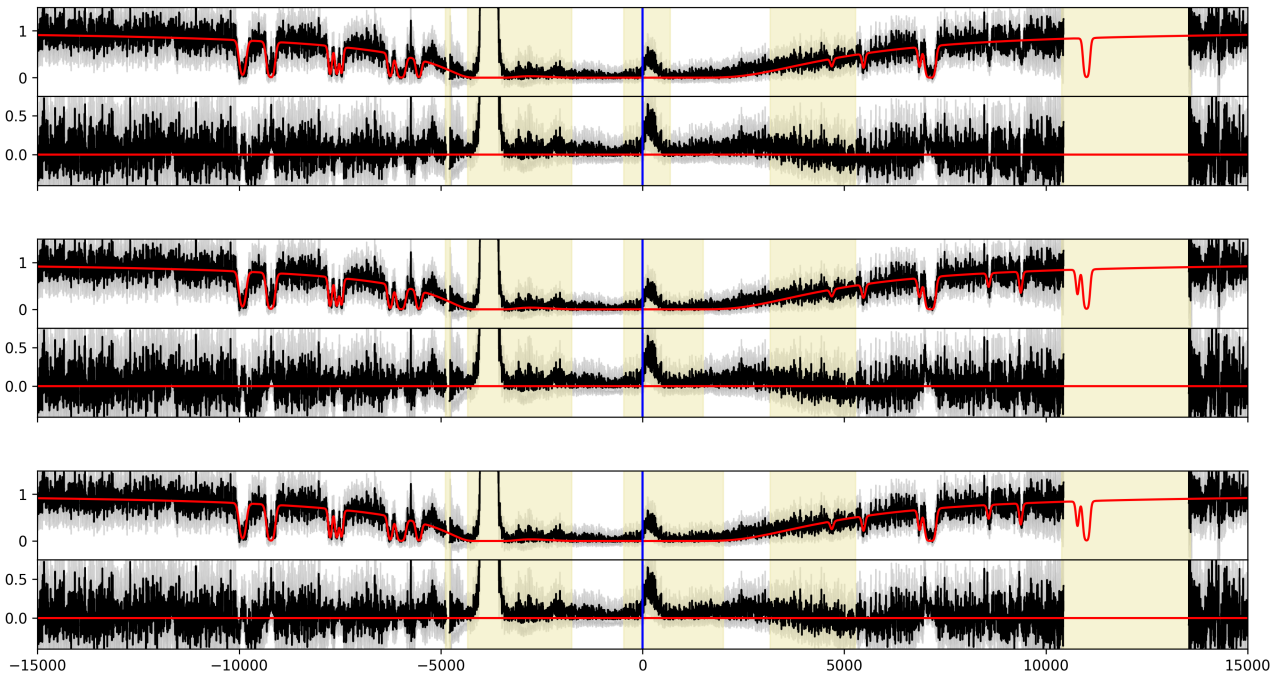

FIG. 7: Galaxy J1044+0353 with z = 0.01287 with fit using free MW H I component.

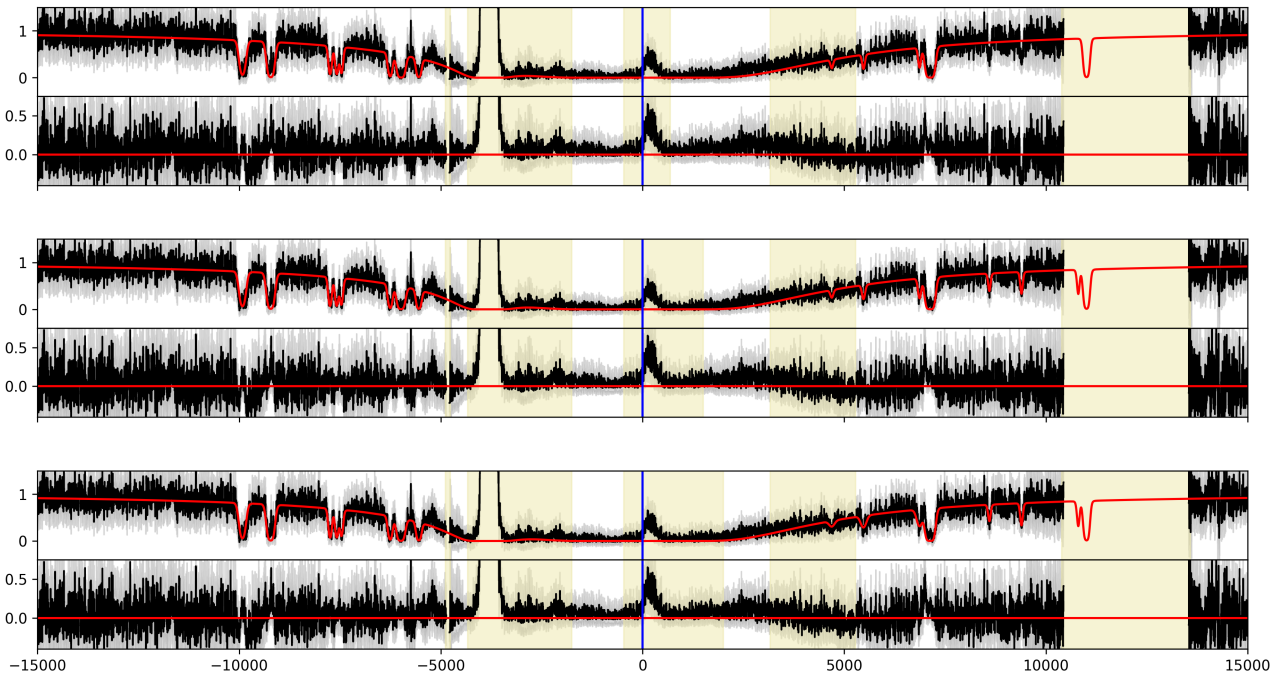

FIG. 8: Galaxy J1044+0353 with z = 0.01287 with fit using free MW H I component.

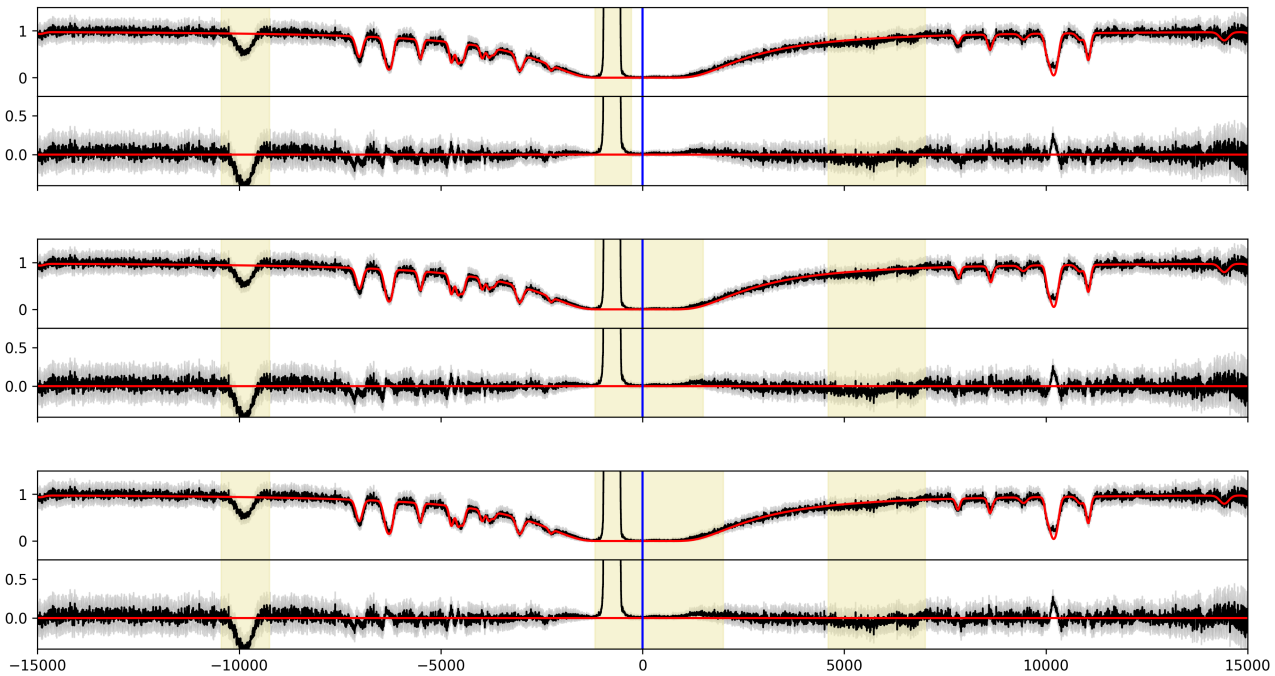

FIG. 9: Galaxy J0934+5514 with z = 0.0025 with fit using fixed MW H I component.

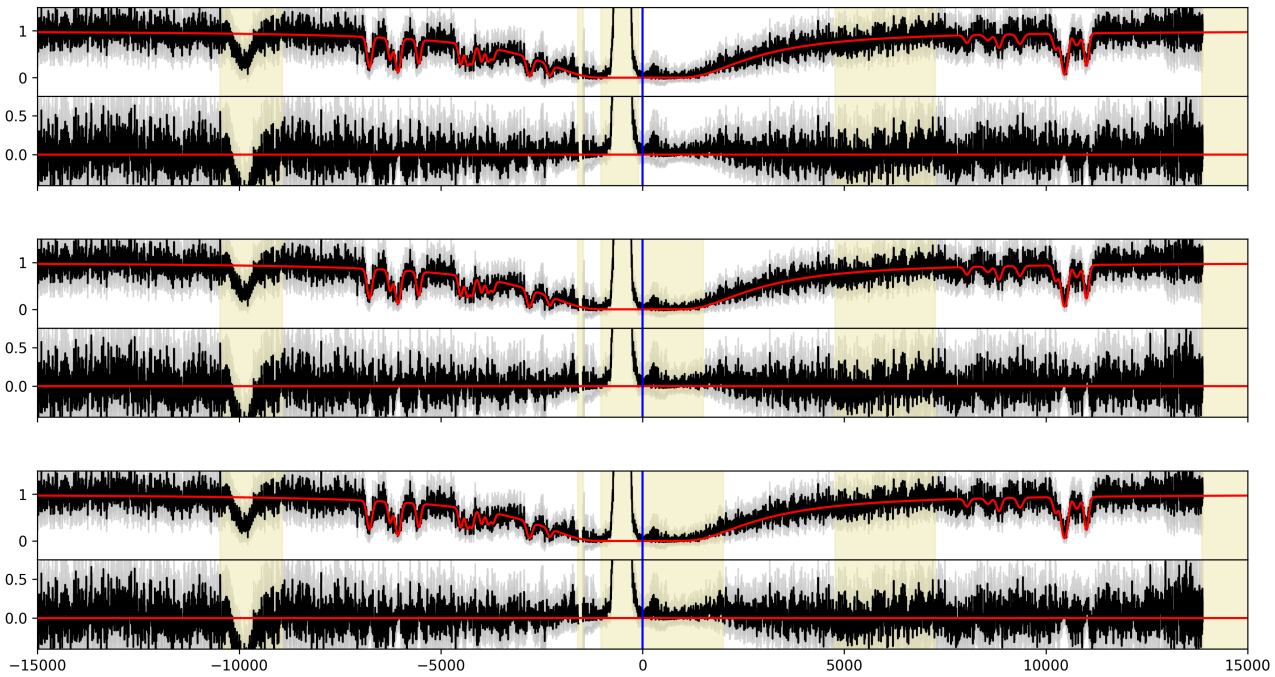

FIG. 10: Galaxy J0940+2935 with z = 0.001675 with fit using fixed MW H I component.

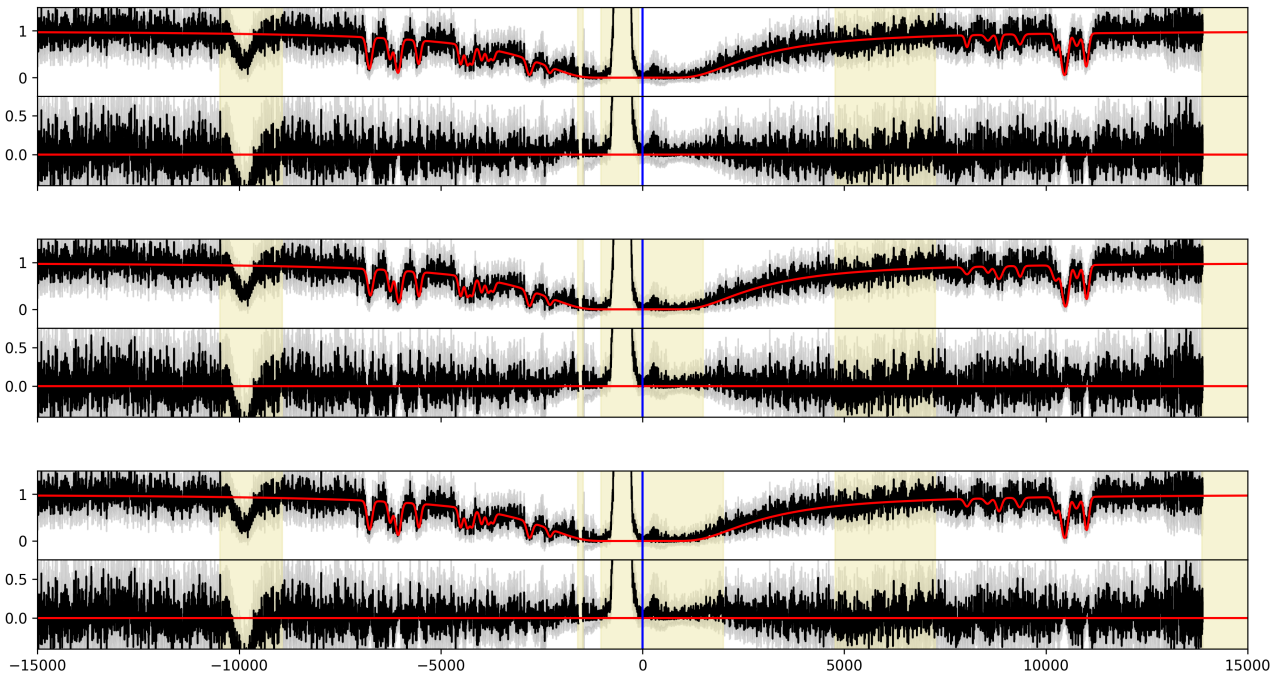

FIG. 11: Galaxy J0940+2935 with z = 0.001675 with fit using free MW H I component.

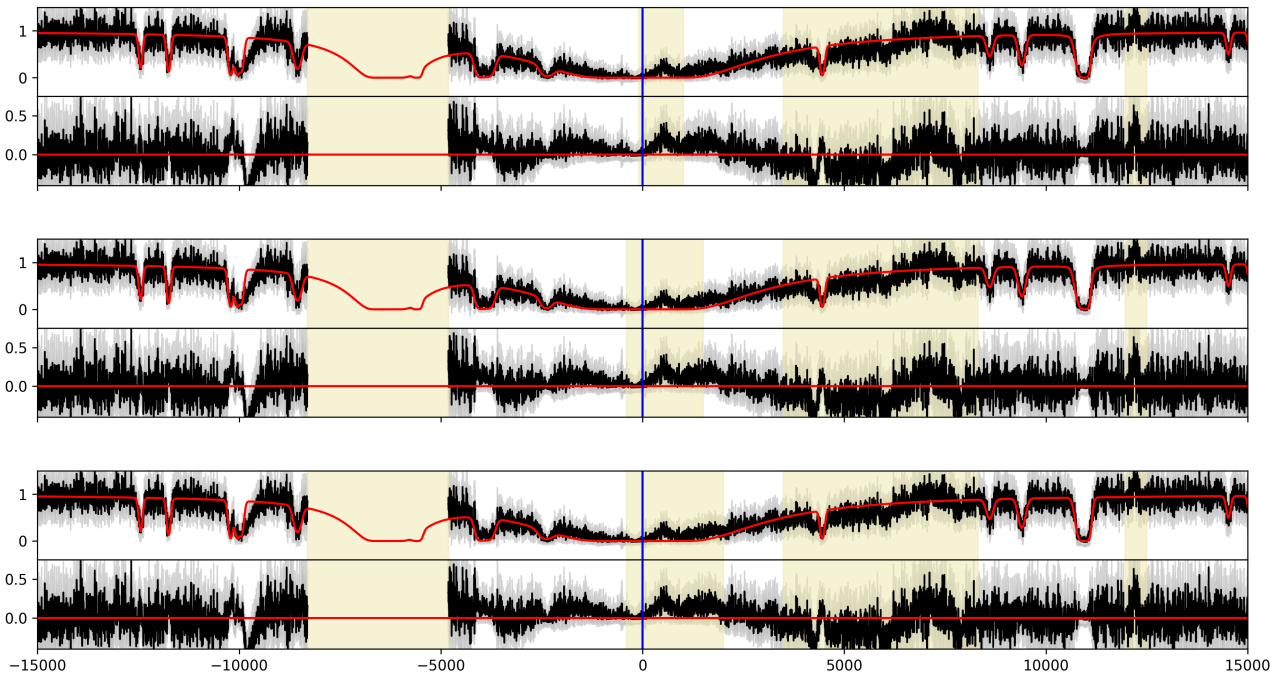

FIG. 12: Galaxy J1105+4444 with z = 0.02154 with fit using fixed MW H I component.

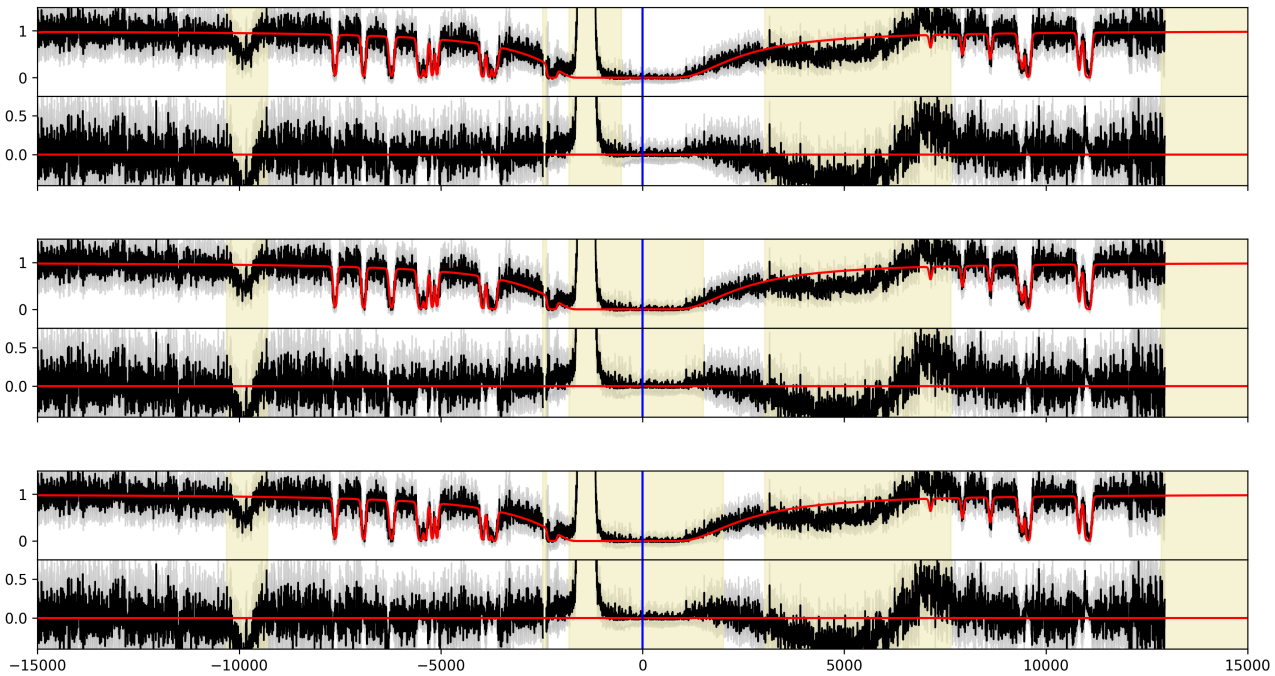

FIG. 13: Galaxy J1129+2034 with z = 0.004703 with fit using fixed MW H I component.

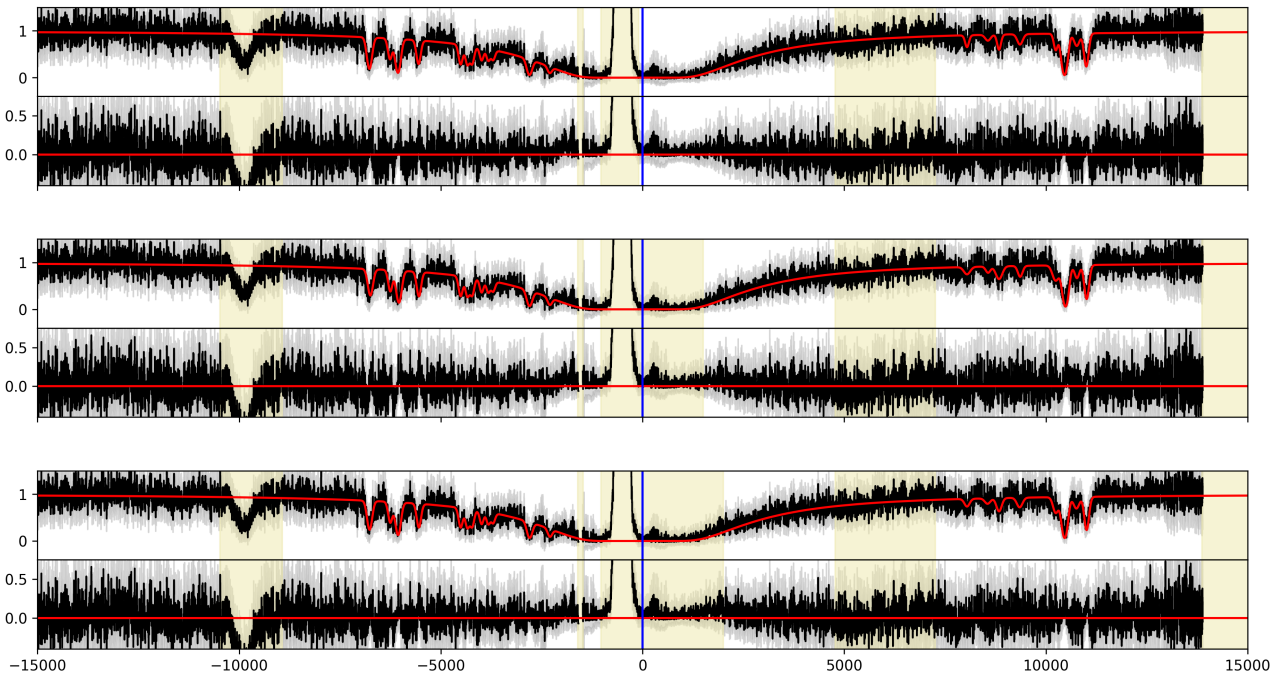

FIG. 14: Galaxy J1129+2034 with z = 0.004703 with fit using free MW H I component.

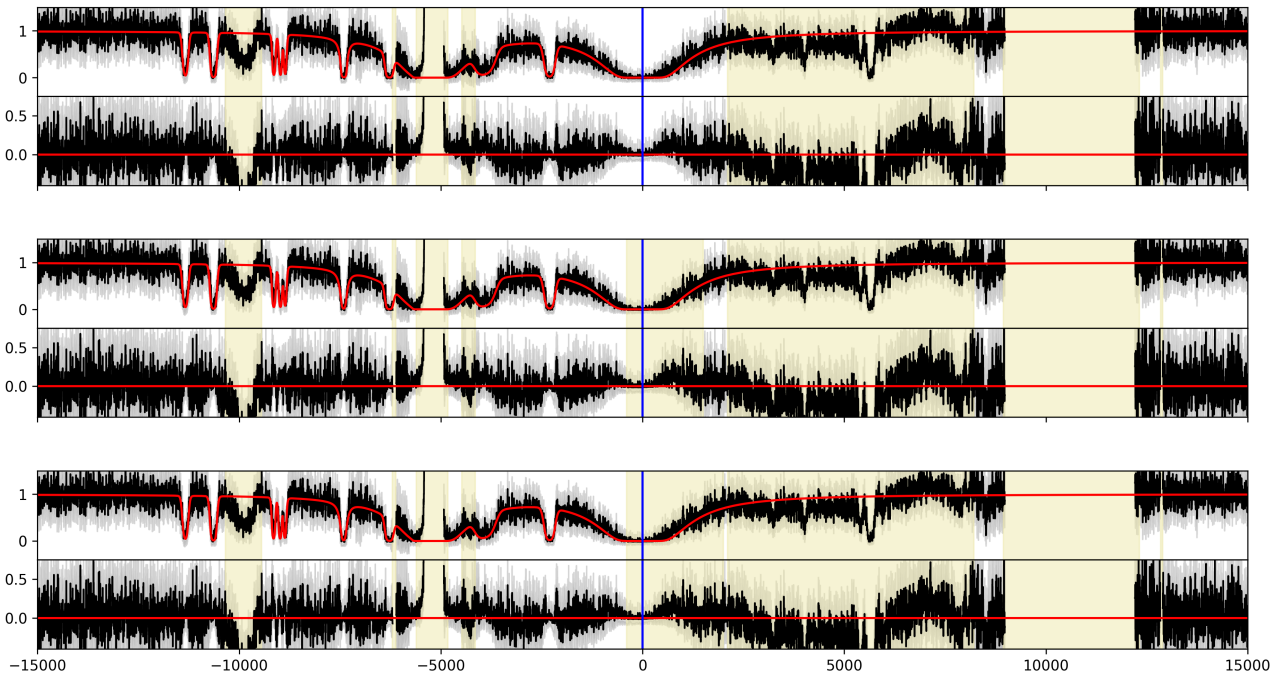

FIG. 15: Galaxy J1132+1411 with z = 0.017637 with fit using fixed MW H I component.

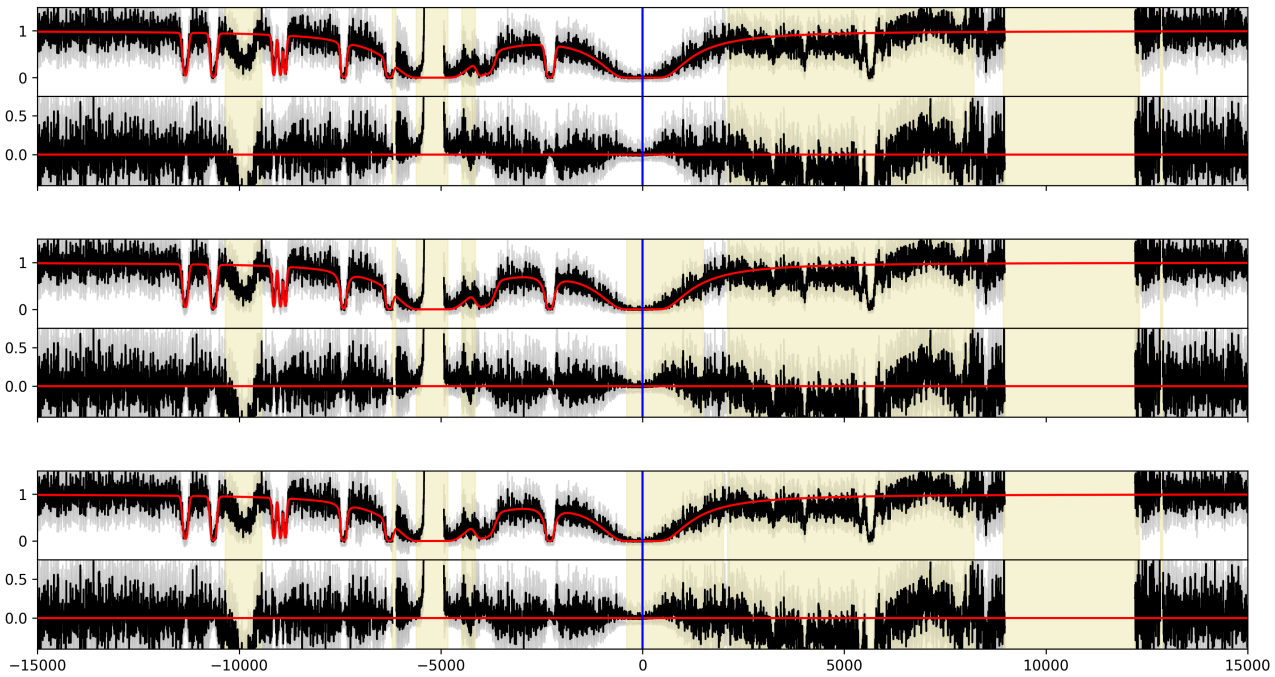

FIG. 16: Galaxy J1132+1411 with z = 0.017637 with fit using free MW H I component.

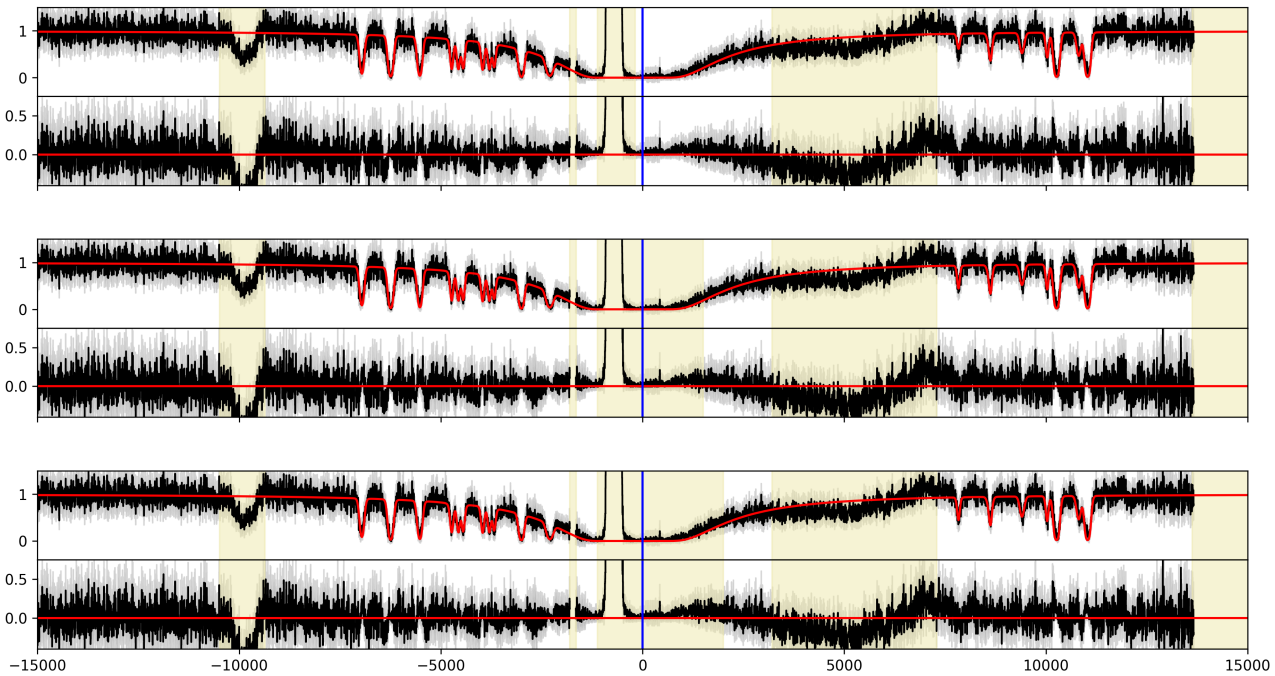

FIG. 17: Galaxy J1150+1501 with z = 0.002448 with fit using fixed MW H I component.

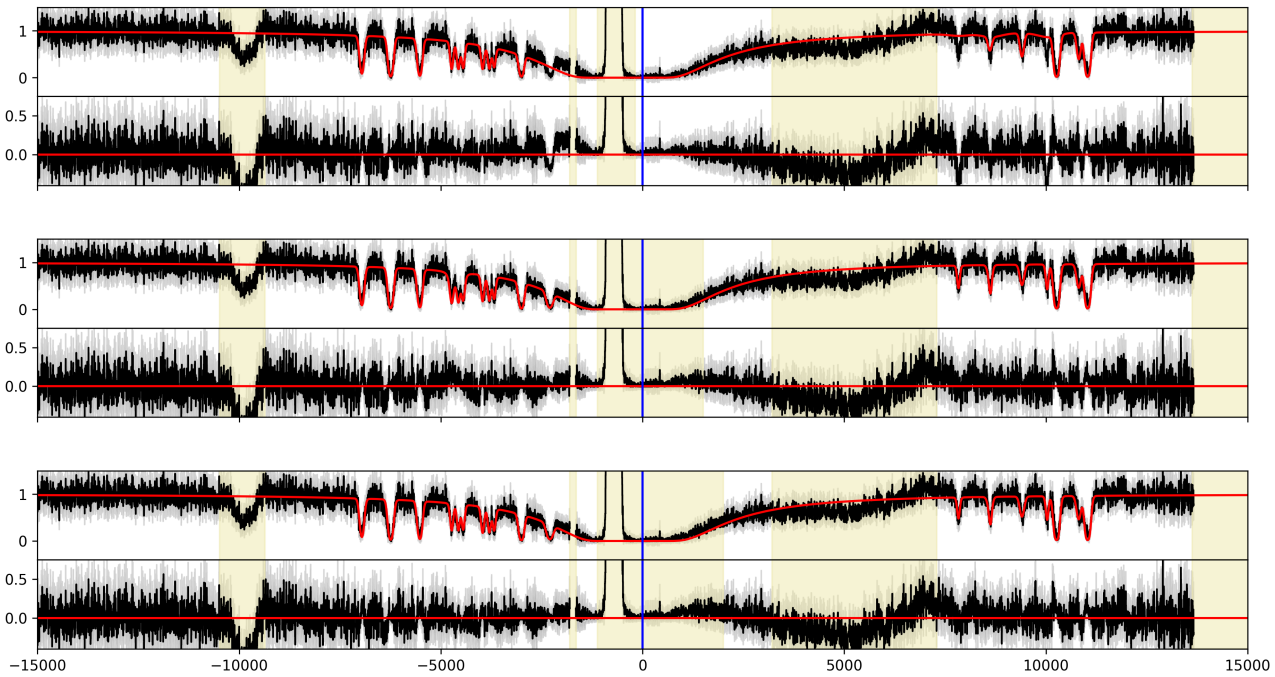

FIG. 18: Galaxy J1150+1501 with z = 0.002448 with fit using free MW H I component.

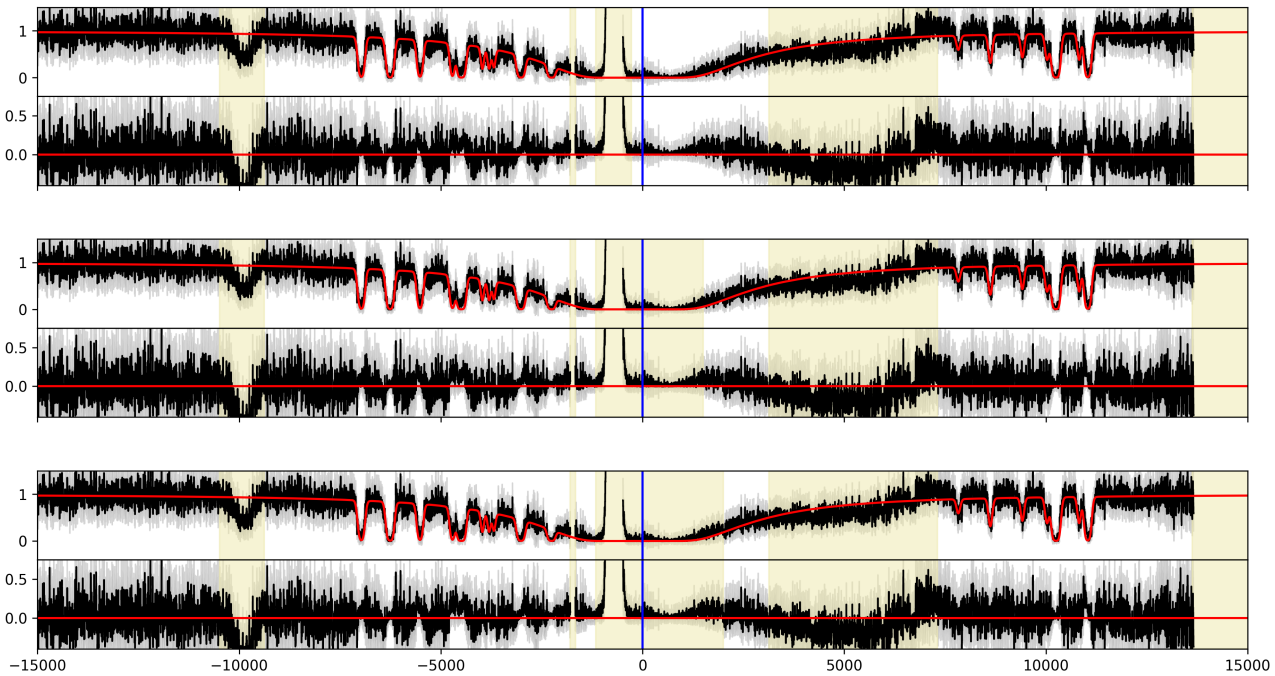

FIG. 19: Galaxy J1225+6109 with z = 0.002341 with fit using fixed MW H I component.

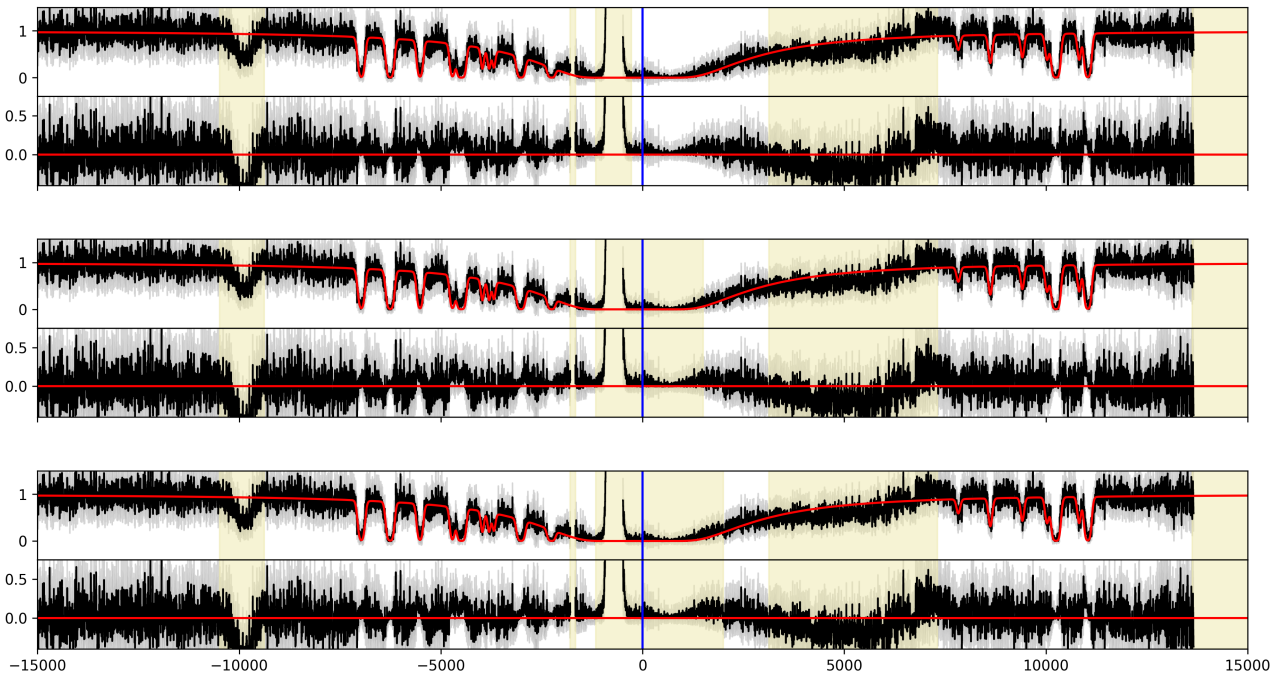

FIG. 20: Galaxy J1225+6109 with z = 0.002341 with fit using free MW H I component.

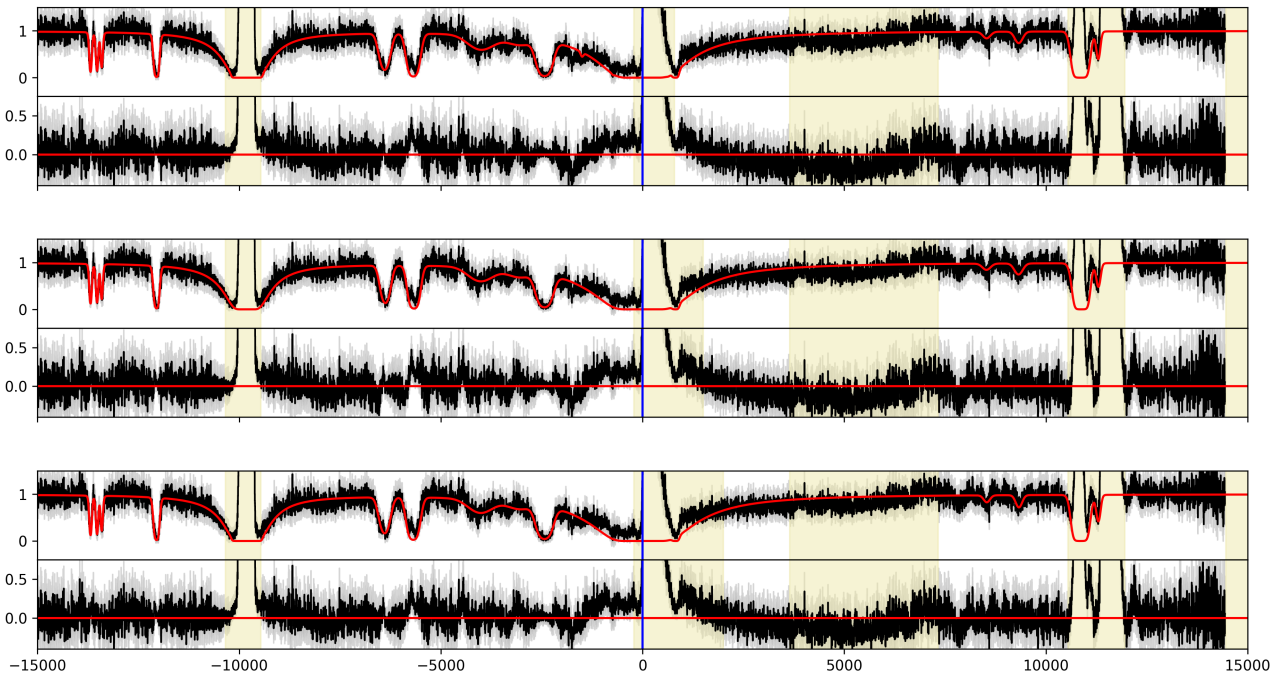

FIG. 21: Galaxy J1359+5726 with z = 0.0033829 with fit using fixed MW H I component.

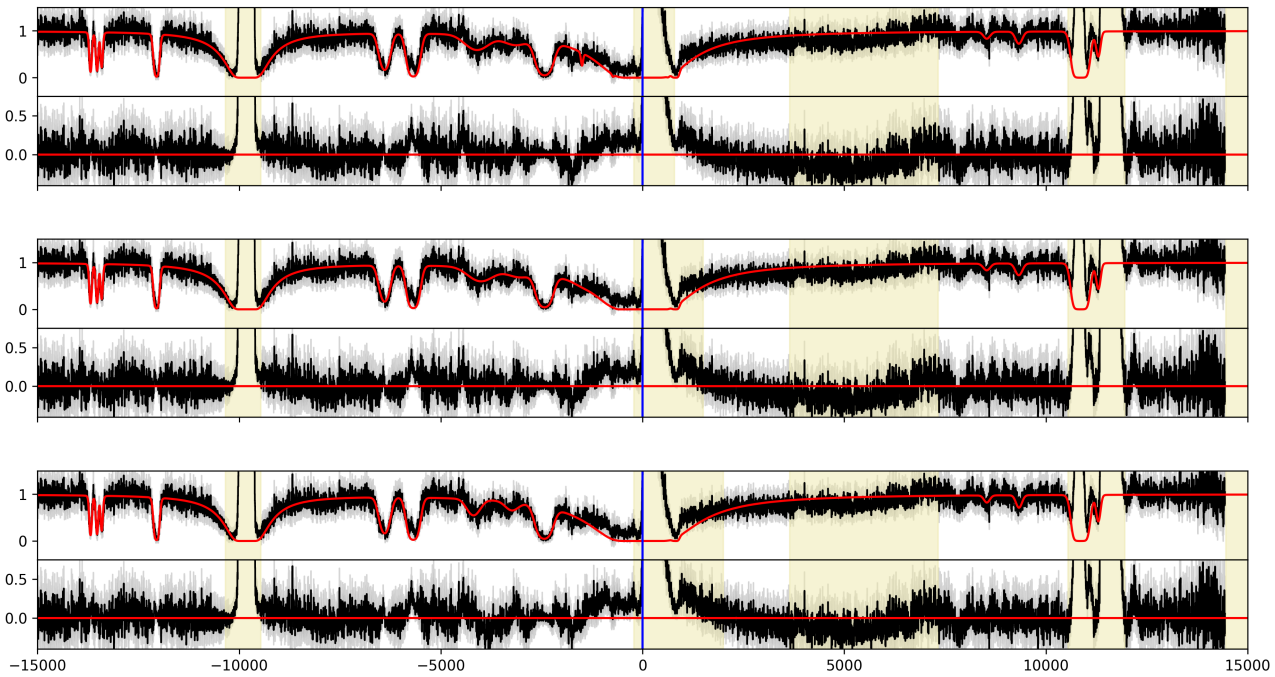

FIG. 22: Galaxy J1359+5726 with z = 0.0033829 with fit using free MW H I component.

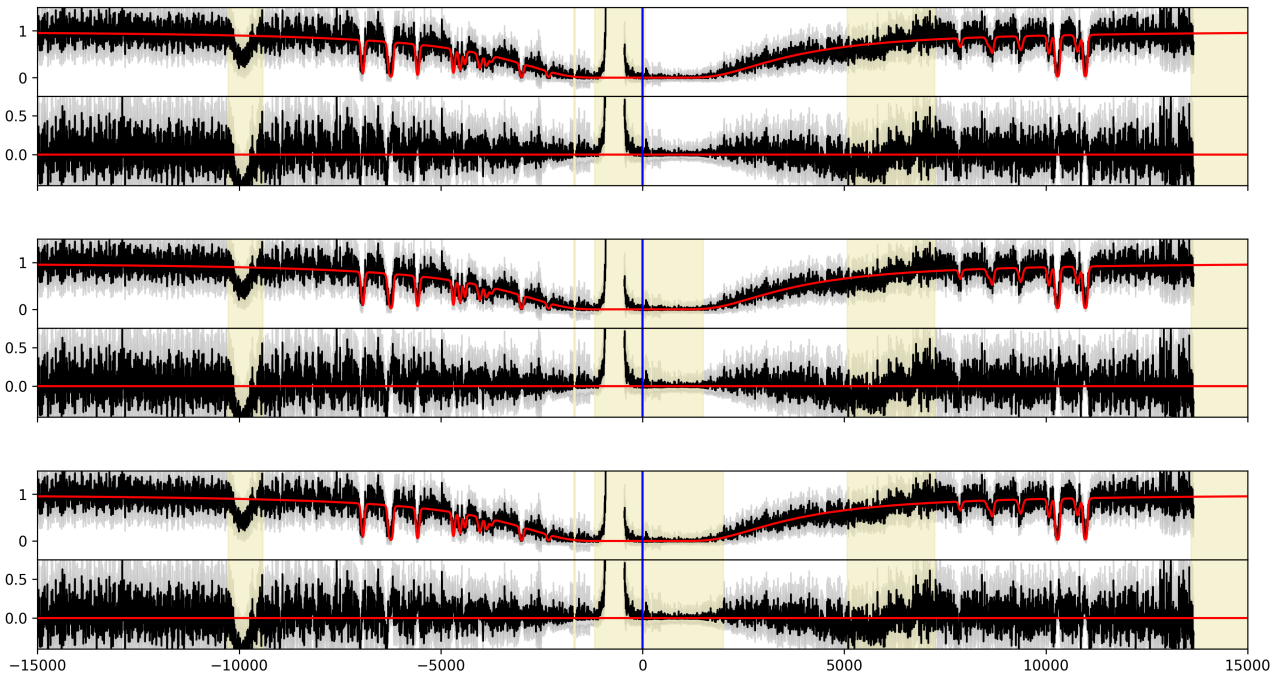

FIG. 23: Galaxy J1444+4237 with z = 0.0023 with fit using fixed MW H I component.

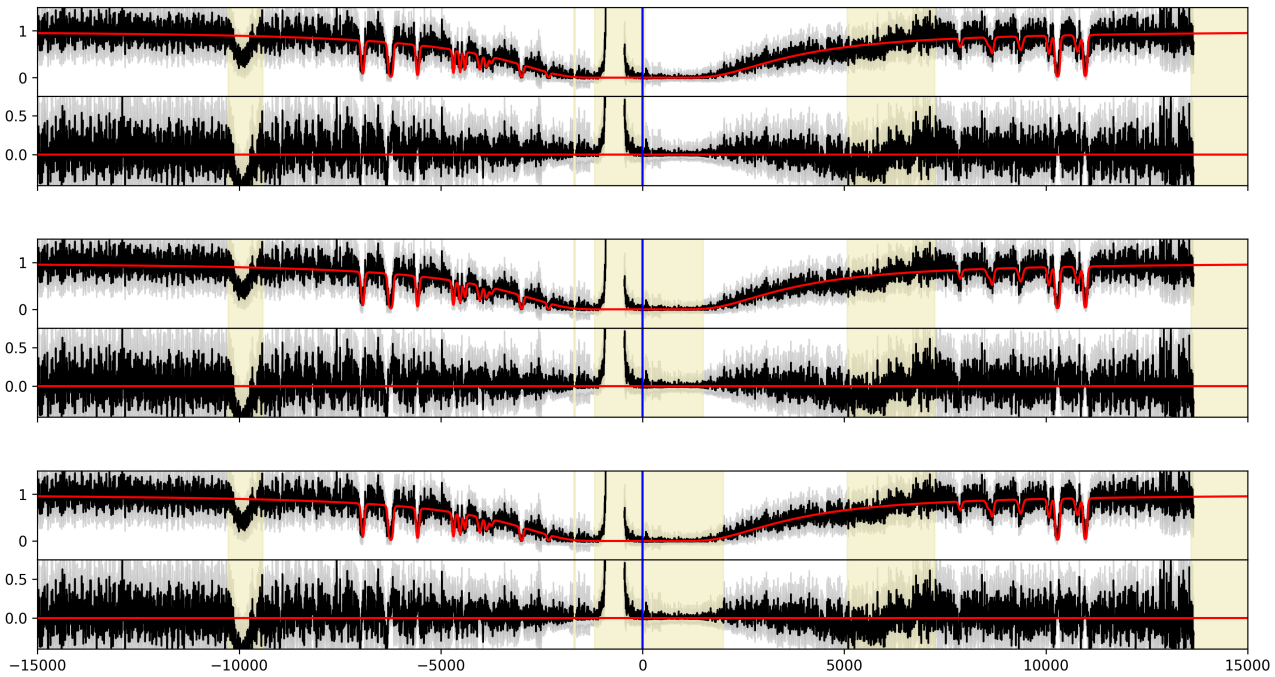

FIG. 24: Galaxy J1444+4237 with z = 0.0023 with fit using free MW H I component.

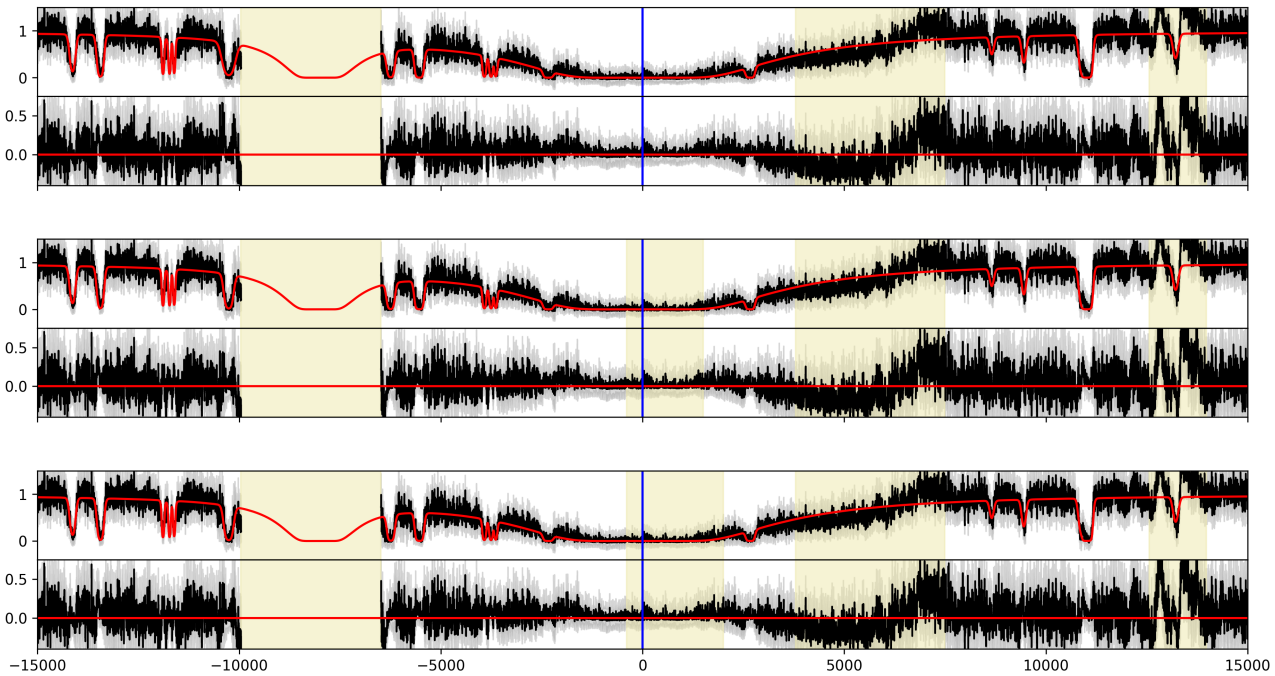

FIG. 25: Galaxy J1448-0110 with z = 0.027412 with fit using fixed MW H I component.